Global Biogeochemical Cycles®

RESEARCH ARTICLE
10.1029/2022GB007316

Nutrient and Silicon Isotope Dynamics in the Laptev Sea and Implications for Nutrient Availability in the Transpolar Drift

G. Laukert[1,2,3], P. Grasse[1,4], A. Novikhin[5], V. Povazhnyi[5], K. Doering[1,6], J. Hölemann[7], M. Janout[7], D. Bauch[1,8], H. Kassens[1], and M. Frank[1]

[1]GEOMAR Helmholtz Centre for Ocean Research, Kiel, Germany, [2]Department of Oceanography, Dalhousie University, Halifax, NS, Canada, [3]Woods Hole Oceanographic Institution, Woods Hole, MA, USA, [4]German Centre for Integrative Biodiversity Research (iDiv) Halle-Jena-Leipzig, Leipzig, Germany, [5]AARI, Arctic and Antarctic Research Institute, Saint Petersburg, Russia, [6]Department of Geology, Lund University, Lund, Sweden, [7]Alfred Wegener Institute, Helmholtz Centre for Polar and Marine Research, Bremerhaven, Germany, [8]Christian-Albrecht University of Kiel, Kiel, Germany

Abstract Realistic prediction of the near-future response of Arctic Ocean primary productivity to ongoing warming and sea ice loss requires a mechanistic understanding of the processes controlling nutrient bioavailability. To evaluate continental nutrient inputs, biological utilization, and the influence of mixing and winter processes in the Laptev Sea, the major source region of the Transpolar Drift (TPD), we compare observed with preformed concentrations of dissolved inorganic nitrogen (DIN) and phosphorus (DIP), silicic acid (DSi), and silicon isotope compositions of DSi ($\delta^{30}Si_{DSi}$) obtained for two summers (2013 and 2014) and one winter (2012). In summer, preformed nutrient concentrations persisted in the surface layer of the southeastern Laptev Sea, while diatom-dominated utilization caused intense northward drawdown and a pronounced shift in $\delta^{30}Si_{DSi}$ from +0.91 to +3.82‰. The modeled Si isotope fractionation suggests that DSi in the northern Laptev Sea originated from the Lena River and was supplied during the spring freshet, while riverine DSi in the southeastern Laptev Sea was continuously supplied during the summer. Primary productivity fueled by river-borne nutrients was enhanced by admixture of DIN- and DIP-rich Atlantic-sourced waters to the surface, either by convective mixing during the previous winter or by occasional storm-induced stratification breakdowns in late summer. Substantial enrichments of DSi (+240%) and DIP (+90%) beneath the Lena River plume were caused by sea ice-driven redistribution and remineralization. Predicted weaker stratification on the outer Laptev Shelf will enhance DSi utilization and removal through greater vertical DIN supply, which will limit DSi export and reduce diatom-dominated primary productivity in the TPD.

Plain Language Summary Ongoing warming and sea ice loss in the Arctic Ocean may significantly impact biological productivity, which is mainly controlled by light and nutrient availability. To investigate nutrient inputs from land, biological utilization, and the influence of water mass mixing and winter processes on the nutrient distributions, we measured nutrient concentrations and silicon isotopes in the Laptev Sea. We found high concentrations in the southeastern Laptev Sea in agreement with nutrient inputs from the Lena River. Toward the northern Laptev Sea, nutrient concentrations decreased in the surface layer and the silicon isotope signatures shifted to heavier values, consistent with nutrient utilization by phytoplankton. In contrast to the depleted surface layer, the bottom layer beneath the Lena River plume was strongly enriched in some nutrients, which we attribute to different physical and biogeochemical processes. These observations are important for our understanding of nutrient bioavailability in the Laptev Sea and the Transpolar Drift (TPD), which is a surface current that connects the Laptev Sea with the central Arctic Ocean and the Fram Strait. The changing hydrography of the Laptev Sea will likely cause a decrease in silicic acid concentrations and thus a reduction in nutrient export and diatom-dominated primary productivity in the TPD.

Key Points:

- Surface dissolved inorganic nitrogen (DIN), dissolved inorganic phosphorus (DIP), silicic acid (DSi), and Si isotope dynamics are controlled by marine and riverine inputs and uptake by phytoplankton
- Strong DIP and DSi enrichments beneath the Lena River plume are due to sea ice-driven nutrient redistribution and remineralization
- Enhanced DSi utilization in the Laptev Sea will lead to a reduced diatom-dominated primary productivity in the Transpolar Drift

Supporting Information:

Supporting Information may be found in the online version of this article.

Correspondence to:

G. Laukert,
georgi.laukert@dal.ca

Citation:

Laukert, G., Grasse, P., Novikhin, A., Povazhnyi, V., Doering, K., Hölemann, J., et al. (2022). Nutrient and silicon isotope dynamics in the Laptev Sea and implications for nutrient availability in the transpolar drift. *Global Biogeochemical Cycles*, *36*, e2022GB007316. https://doi.org/10.1029/2022GB007316

Received 14 JAN 2022
Accepted 31 AUG 2022

Author Contributions:

Conceptualization: A. Novikhin, J. Hölemann, H. Kassens, M. Frank
Data curation: P. Grasse, A. Novikhin, V. Povazhnyi, K. Doering
Funding acquisition: H. Kassens, M. Frank
Investigation: P. Grasse, A. Novikhin, V. Povazhnyi, K. Doering, J. Hölemann, M. Janout, D. Bauch, H. Kassens, M. Frank

1. Introduction

Sea ice loss, freshening, and stratification changes driven by global warming in the recent past have already affected, and are projected to continue to affect, the seasonal timing and distribution of primary productivity in the Arctic Ocean (IPCC, 2022). In the photic layer, primary productivity is ultimately limited by nutrient availability and hence regulated by vertical and lateral nutrient supply. On a pan-Arctic scale, replenishment of surface water macronutrient levels (*here*: dissolved inorganic nitrogen, DIN; dissolved inorganic phosphorus, DIP; and silicic acid, DSi) from the deep pool via vertical mixing is the main process governing primary productivity (Hill

Methodology: P. Grasse, A. Novikhin, V. Povazhnyi, K. Doering, J. Hölemann, M. Janout, D. Bauch, M. Frank
Project Administration: H. Kassens, M. Frank
Supervision: M. Frank
Validation: P. Grasse, M. Frank
Writing – review & editing: P. Grasse, A. Novikhin, V. Povazhnyi, K. Doering, J. Hölemann, M. Janout, D. Bauch, H. Kassens, M. Frank

et al., 2013; Randelhoff et al., 2020). In the extensive Arctic shelf areas, terrigenous nutrient inputs from land and nutrient cycling exert additional strong controls on nutrient bioavailability, supporting as much as one third of the current net primary productivity in the Arctic Ocean (Terhaar et al., 2021). In some of these marginal regions, despite the decrease in sea ice cover and opposite to the general trend, primary productivity has decreased in the recent past (Ardyna & Arrigo, 2020; Arrigo & van Dijken, 2015; Demidov et al., 2020; Lewis et al., 2020). While it is unclear how this inconsistent response of primary productivity is linked to changes in stratification, nutrient supply, and cycling, it demonstrates that a deep understanding of the complex balance between these controlling mechanisms in Arctic shelf regions is critical for predicting future changes in ecosystem functioning. Large parts of the Arctic Ocean are affected by waters and nutrients exported from these regions, indicating a regional and a large-scale, pan-Arctic influence on marine biogeochemistry and biology.

The Laptev Sea is the main source region of the Transpolar Drift (TPD) and is among the peripheral Arctic regions most affected by climate change. Therefore, it is also a key region for investigations of nutrient biogeochemistry on the Siberian Shelf. The Laptev Sea connects the Kara and East Siberian Seas while at the same time receiving large amounts of freshwater from the Lena River and marine waters of Atlantic origin (Figure 1). Freshwater and dense bottom waters originating from the Laptev Sea feed into the TPD (Paffrath et al., 2021) and maintain the Arctic halocline (Bauch et al., 2011, 2014; Janout et al., 2015), respectively, while at the same time transporting dissolved and particulate constituents including nutrients and trace elements to the central Arctic Ocean (e.g., Bauch et al., 2011; Charette et al., 2020; Klunder et al., 2012; Laukert, Frank, Bauch, Hathorne, Gutjahr et al., 2017, Laukert, Frank, Bauch, Hathorne, Rabe et al., 2017; Middag et al., 2011; Paffrath et al., 2021; Rijkenberg et al., 2018; Slagter et al., 2017). The highly variable hydrography of the Laptev Sea is the result of changes in atmospheric circulation, strong seasonality in river discharge, and the formation, melting, and export of sea ice (Janout et al., 2013, 2015, 2016, 2020). The surface layer of the central and eastern Laptev Sea is dominated by Lena River freshwater, which is responsible for a year-round stratification except for a short period of time before the seasonal ice retreat in spring (Janout et al., 2020). The northwestern Laptev Sea, in contrast, is mainly influenced by waters from the Kara Sea (Janout et al., 2015; Laukert, Frank, Bauch, Hathorne, Gutjahr et al., 2017) and is well-mixed from mid-December to sea ice breakup in spring (Janout et al., 2016, 2020). Since the mid-2000s, the Laptev Sea shelf has been ice-free in summer as a function of overall higher temperatures, resulting in enhanced hydrographic variability and tentatively weaker stratification due to stronger atmosphere-ocean coupling (Janout et al., 2020). This observation contrasts with expectations of increasing stratification due to sea ice loss and warming, highlighting the need to better constrain nutrient dynamics in this region and their impact on nutrient bioavailability in the TPD.

Numerous investigations have focused on the mechanisms controlling the distribution and bioavailability of macronutrients and micronutrients in the Laptev Sea (e.g., Bauch & Cherniavskaia, 2018; Bauch et al., 2014; Cauwet & Sidorov, 1996; Codispoti & Richards, 1968; Gordeev & Sidorov, 1993; Gordeev et al., 1996; Kattner et al., 1999; Klunder et al., 2012; Létolle et al., 1993; Martin et al., 1993; Nitishinsky et al., 2007; Sanders et al., 2022; Sorokin & Sorokin, 1996; Sun et al., 2021; Thibodeau et al., 2017). Most of these studies were based on nutrient concentration data, which in combination with salinity and other hydrographic parameters were used to assess nutrient input from external sources, conservative mixing, biological uptake, and remineralization. Pioneering investigations identified the Lena River as the main source of riverine inorganic nutrients to the Laptev Sea and found strong contrasts in nutrient concentrations between surface and bottom waters near the Lena Delta in summer (Cauwet & Sidorov, 1996; Codispoti & Richards, 1968; Létolle et al., 1993). More recently, erosion of coastal soils was suggested to be another strong source of terrestrial nutrients to the water column (Fritz et al., 2017; Holmes et al., 2012; Sanders et al., 2022; Terhaar et al., 2019, 2021). The widely observed depletion of nutrients in the freshwater enriched surface layer has been attributed to water mass mixing and biological utilization by primary producers (Codispoti & Richards, 1968; Gordeev et al., 1996; Kattner et al., 1999; Létolle et al., 1993). The average annual primary productivity was recently reestimated at 125 mg C/m^2 per day for the entire Laptev Sea and maximum productivity rates were observed from May to July (Demidov et al., 2021). In situ remineralization of organic matter and associated nutrient release were invoked to explain high concentrations particularly of DIP and DSi in the bottom layer (Cauwet & Sidorov, 1996; Codispoti & Richards, 1968; Létolle et al., 1993; Nitishinsky et al., 2007). Some DSi concentrations reported for bottom waters in the Lena estuary, however, exceeded the maximum amount attributable to phytoplankton decomposition (Codispoti & Richards, 1968), hinting at additional processes supplying nutrients to the water column. Thibodeau et al. (2017) suggested atmospheric nitrogen inputs to the bottom layer through admixture of brine-enriched dense waters

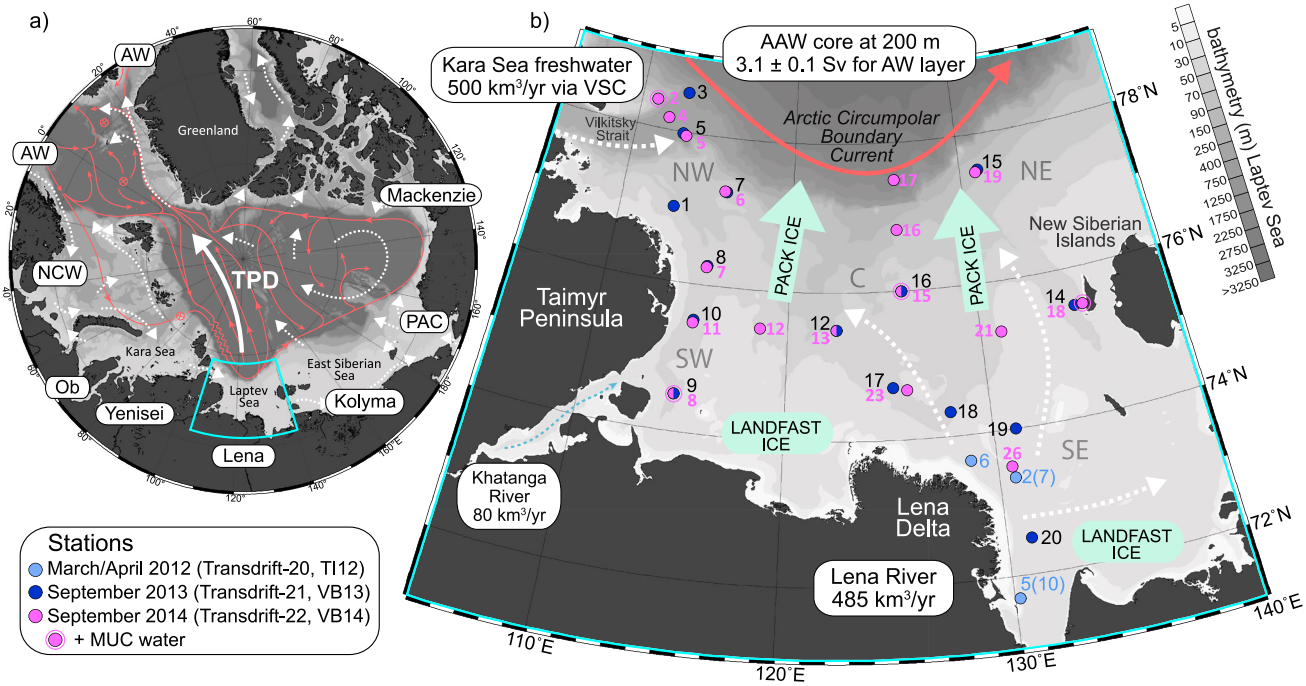

Figure 1. (a) Bathymetric map of the Arctic Mediterranean (i.e., Nordic Seas and Arctic Ocean) with circulation scheme of surface currents (dashed white arrows), the Transpolar Drift (TPD, solid white arrow), and subsurface Atlantic and intermediate layers (solid red arrows) (modified after Rudels et al. (2012)) and the major riverine and marine nutrient sources (AW = Atlantic-derived water; NCW = Norwegian Coastal Water, and PAC = Pacific-derived water). The area shown in (b) is highlighted in turquoise. (b) Laptev Sea region with the Arctic Boundary Current (mean volume transport at 125°E is from Pnyushkov et al. (2021) and given in Sverdrup (Sv, in 10^6 m^3/s)) and potential freshwater pathways (mean annual freshwater transport for the Khatanga and Lena rivers is taken from R-ArcticNET http://www.r-arcticnet.sr.unh.edu/ and for Kara Sea freshwater advected via the Vilkitsky Strait Current is taken from Janout et al. (2015)). Arctic Atlantic Water is modified AW at ~200 m depth. Stations of this study (only for *isotope samples*, see main text) are shown as color coded symbols and station numbers. In addition to seawater samples recovered above and below the pycnocline, bottom water samples immediately above the undisturbed sediment-water interface were recovered at four stations in 2014 using a multicorer device.

formed during seasonal sea ice growth. This winter process likely also affects the distribution of other dissolved organic and inorganic constituents in the Laptev Sea (e.g., Bauch et al., 2011; Hölemann et al., 2021; Laukert, Frank, Bauch, Hathorne, Gutjahr et al., 2017).

The fate of terrigenous nutrients such as those introduced to the Laptev Sea through the various Siberian rivers has been discussed on the pan-Arctic scale (Le Fouest et al., 2013; Torres-Valdés et al., 2013). A net export of DSi and DIP from the Arctic Ocean to the North Atlantic has been determined and has been attributed to riverine input sources in the case of DSi (Torres-Valdés et al., 2013). In contrast, the DIN budget was assumed to be balanced, supporting the observation of widespread DIN limitation in the Arctic Ocean (e.g., Tremblay & Gagnon, 2009; Tremblay et al., 2012, 2015) under the assumption that most of the utilized DIN is eventually regenerated in the water column and exported from the Arctic Ocean (Macdonald et al., 2010). DSi excess and DIN limitation are consistent with low removal rates (~14%) of riverine DSi by phytoplankton when only riverine DIN is consumed (Le Fouest et al., 2013). However, diatom-dominated primary productivity in some regions of the Atlantic sector of the Arctic Ocean may also strongly deplete DSi due to a continuous supply of DIN from the deep pool (Codispoti et al., 2013; Duarte et al., 2021; Giesbrecht & Varela, 2021; Krause et al., 2019; Krisch et al., 2020; Sakshaug, 2004; Wheeler et al., 1997). In addition to the DSi-rich but DIN-poor "shelf-influenced" and the DSi-poor but DIN-rich "Atlantic" regimes, enhanced diatom productivity can establish a "Polar" regime with very low DSi and DIN concentrations (e.g., Fernández-Méndez et al., 2015; Flores et al., 2019). The distribution of these regimes is strongly linked to upper ocean circulation in addition to primary productivity and hence subject to the influence of near-surface currents such as the TPD. Recently, Paffrath et al. (2021) identified two laterally and vertically separated source freshwater clusters within the TPD, corresponding to shelf waters with dominating freshwater contributions either from the Lena River (Lena domain) or the Yenisei and Ob rivers (Yenisei/Ob domain). Both domains mainly originate in the Laptev Sea, their current and future role in

establishing and sustaining the various nutrient regimes therefore highly depends on the Laptev Sea's spatiotemporally variable hydrology and biogeochemistry.

The biogeochemistry of Si is of particular importance for biological productivity in the Laptev Sea, given that diatoms, the main primary producers consuming DSi, currently dominate the phytoplankton composition (Cremer, 1999; Fahl et al., 2001; Tuschling, 2000). In the near future, the DSi supply from land to the Arctic Ocean may increase due to enhanced weathering and riverine inputs (Tréguer et al., 2021 and references therein). However, the potential impact of this increase on primary productivity and hence the biological pump is unclear. In addition to nutrient concentrations, stable silicon (Si) isotope compositions of DSi (expressed as $\delta^{30}Si_{DSi}$) may provide further information on Si sources, utilization, and cycling (e.g., Sutton et al., 2018) given that Si isotopes are fractionated during diatom growth due to preferential incorporation of the light isotopes into the diatom frustules (de la Rocha et al., 1997). To date no $\delta^{30}Si_{DSi}$ data have been reported for the Siberian Interior Shelf Seas (i.e., the Kara, Laptev, and East Siberian Seas) but $\delta^{30}Si_{DSi}$ distributions in other shallow and deep regions of the Arctic Ocean confirm the viability of Si isotopes to trace Si utilization and cycling in the northern high latitudes (Brzezinski et al., 2021; Debyser et al., 2022; Giesbrecht et al., 2022; Liguori et al., 2020, 2021; Varela et al., 2016). Recently, Brzezinski et al. (2021) and Liguori et al. (2021) reported relatively high DSi concentrations accompanied by heavy $\delta^{30}Si_{DSi}$ values for TPD waters, which they attributed to riverine DSi inputs on the Siberian Shelf and biological DSi utilization. The combination of these processes could also explain similar DSi-$\delta^{30}Si_{DSi}$ characteristics in the East Greenland Current at Fram Strait, consistent with the export of DSi from the Siberian Interior Shelf Seas to the North Atlantic (Debyser et al., 2022). Brzezinski et al. (2021) also presented a preliminary Si isotope budget for the Arctic Ocean, which is only balanced if effective burial of frustules with exceptionally light $\delta^{30}Si$ occurs on the shelves. The $\delta^{30}Si_{DSi}$ signatures of the marine (Brzezinski et al., 2021; Liguori et al., 2020, 2021; Varela et al., 2016) and riverine (Mavromatis et al., 2016; Pokrovsky et al., 2013; Sun et al., 2018) DSi sources contributing to the Laptev Sea are well constrained. Therefore, an important condition for verifying the above assumptions and for studying the Si biogeochemical cycle based on $\delta^{30}Si_{DSi}$ signatures is fulfilled for the Laptev Sea.

In this study, we investigate the impacts of external nutrient inputs, conservative mixing and nutrient utilization, and cycling on nutrient distributions in the Laptev Sea with a specific focus on the biogeochemical cycle and the isotopic distribution of Si, based on samples recovered in winter 2012 and the summers of 2013 and 2014 (Figure 1). To determine nonconservative nutrient changes (i.e., changes beyond *preformed* values expected from external nutrient inputs and conservative mixing), we employed a water component analysis established previously for the same years and samples (Laukert, Frank, Bauch, Hathorne, Gutjahr et al., 2017). Based on the calculated changes in nutrient concentrations and $\delta^{30}Si_{DSi}$ from preformed to measured values, we suggest that combined external inputs, seasonal hydrographic changes, and biological and biogeochemical processes significantly affect nutrient distributions in the Laptev Sea. Anticipated near-future changes in these distributions will have strong implications for nutrient export to and nutrient bioavailability in the TPD.

2. Materials and Methods

2.1. Sample Collection and Treatment of Isotope Samples

All samples reported here were collected during two summer expeditions in 2013 and 2014 (Transdrift 21 and 22, respectively) and during one winter expedition in 2012 (Transdrift 20) (Figure 1). The summer samples were recovered across the entire Laptev Sea shelf and above the shelf slope (down to ~310 m depth) along with CTD (conductivity, temperature, depth) profiles with an SBE 32 rosette water sampler equipped with 12 Niskin bottles (2.5 L) under ice-free conditions on board the Russian research vessel RV Viktor Buynitskiy. Most stations of the 2013 expedition were reoccupied in 2014 enabling direct interannual comparison. Comparing summer and winter data further allows the determination of seasonal variations. Sampling in winter 2012 was conducted with 2 L Niskin-type bottles at three ice camps in the landfast ice area east and northeast of the Lena Delta. Concentrations of DIN ([DIN]), DIP ([DIP]), and DSi ([DSi]) were obtained from small-volume samples recovered at a high vertical resolution (hereafter referred to as *nutrient samples*). In addition, large-volume (10 L) seawater samples were recovered during the two summers and the winter for isotope measurements at the same stations but at a lower resolution, from different casts and at slightly different depths (hereafter referred to as *isotope samples*). Where possible, one isotope sample from the surface mixed layer and one isotope sample from the bottom layer were collected at each station to include waters present above and below the pycnocline. In addition, four bottom

water isotope samples directly above the undisturbed sediment-water interface were recovered in 2014 with a multicorer device (MUC).

Isotope samples collected in the summer of 2013 and 2014 were immediately filtered through AcroPak™500 Capsules containing sequential 0.8/0.2 µm Supor® membrane filters and stored in acid-cleaned LDPE-Cubitainers before they were acidified to pH ~2.2 with ultrapure concentrated HCl at the Otto-Schmidt Laboratory in St. Petersburg, Russia. Samples obtained during the winter expedition in 2012 were treated similarly, except that they were filtered through 0.45 µm Millipore® cellulose acetate filters using a peristaltic pump and subsequently acidified after transport to the home laboratory at GEOMAR, Kiel. Aliquots of the isotope samples have been used to determine selected provenance tracers (neodymium and oxygen isotopes) and dissolved rare earth elements (REEs), whose distribution is reported and discussed by Laukert, Frank, Bauch, Hathorne, Gutjahr et al. (2017). In our study, 0.01–0.1 L aliquots of these geochemically well-characterized samples have been used for the determination of dissolved stable Si isotopes ($\delta^{30}Si_{DSi}$) and the corresponding [DSi]. These aliquots were separated into 1 L acid-cleaned LDPE-bottles and kept in the dark for less than five years before final treatment and analysis (Sections 2.2 and 2.3).

2.2. Nutrient Concentrations

All concentrations presented in this study were measured following the procedures by Grasshoff et al. (1999). Nutrient samples recovered in 2012 and 2013 were frozen at −20°C directly after collection, whereas samples recovered in 2014 were measured directly onboard with a KFK-3 spectrophotometer. Frozen samples (from 2012 to 2013) were transported to the Otto-Schmidt Laboratory in St. Petersburg and nutrient concentrations were analyzed using a Skalar San$^+$ nutrient autoanalyzer. To allow for direct comparison with $\delta^{30}Si_{DSi}$ values [DSi] was remeasured on filtered and acidified subsamples of all (2012, 2013, and 2014) the isotope samples at GEOMAR, Kiel, using a nutrient autoanalyzer system (QuAAtro, SEAL Analytical).

The quality of the nutrient data was ensured by continuous measurements of certified reference material NMIJ CRM 7602a provided by the National Metrology Institute of Japan and in addition assessed by a comparison of concentrations in deeper waters (between 150 and 300 m) with published data from independent surveys conducted in or near the study region (Table S1). At such depths, similar concentrations can be expected due to smaller spatial and temporal variations. For comparison, we used data from samples collected in 2015 along a 125°E Laptev Shelf slope transect (data from the Nansen and Amundsen Basin Observation System II, NABOS-II; https://arcticdata.io) and from the central Arctic Ocean (data from RV POLARSTERN expedition PS94, ARK-XXIX/3, stations 58–134; van Ooijen et al., 2016). Our mean [DIP] and [DSi] are within error identical with the data from these open ocean surveys, while [DIN] on average is lower by ~4 µM for 2013 and by ~2 µM for 2014. Thibodeau et al. (2017) reported [DIN] data from samples used for nitrogen isotope analysis collected independently during the same summer expedition in 2014 that are overall identical within error with our data from the same expedition. In addition, Schulz et al. (2022) recently reported similarly low [DIN] at the Laptev Sea margin for 2018. Therefore, we conclude that the differences observed in [DIN] between the open ocean surveys conducted in 2015 and our surveys in 2013 and 2014 are linked to slight hydrological differences rather than sample treatment and analysis.

In order to allow for an assessment of nutrient distributions based on a water component analysis developed by Laukert, Frank, Bauch, Hathorne, Gutjahr et al. (2017) using the same samples and to enable comparison of the nutrient data with dissolved $\delta^{30}Si_{DSi}$ and other parameters (e.g., dissolved REEs), we linearly interpolated the original high-resolution nutrient data on the isopycnal surfaces based on the two nearest nutrient values above and below each surface (measured and interpolated values are <2 m apart in surface waters and <10 m below the pycnocline). Despite differences observed for individual samples, the interpolated high-resolution [DSi] data agree well ($R^2 = 0.85$) with [DSi] determined in the isotope samples. The differences (up to 50% for individual samples) are likely either caused through nutrient and isotope sample recovery from different casts and at slightly different depths or through reactive DSi loss after frozen storage (Becker et al., 2020), which might have affected the nutrient samples recovered in winter 2012 and summer 2013. To avoid the latter issue, we use [DSi] obtained from the filtered and acidified isotope samples for our water component analysis. Given that [DIN] and [DIP] have not been determined in the isotope samples, a comparison for these nutrients is not possible.

2.3. Silicon Isotopes

The validity of the entire preconcentration, purification, and measurement procedures for dissolved Si isotope analysis applied in our study was confirmed through participation of our laboratory in the international

GEOTRACES Si isotope intercalibration study (Grasse et al., 2017) and is reported in detail in the Supporting Information (Text S1 in Supporting Information S1). In brief, samples were first treated with ultraviolet light (254 and 365 nm, UV hand lamp from Herolab GmbH, reference 2950740) and diluted (0.1%) hydrogen peroxide (H_2O_2) to destroy dissolved organic matter (Hughes et al., 2011). Silicon was preconcentrated applying the magnesium-induced coprecipitation (MAGIC) method using sodium hydroxide based on the method by Karl and Tien (1992) modified by Reynolds et al. (2006) (see also Ehlert et al., 2012; Grasse et al., 2013). The samples were purified chromatographically using a cation exchange resin (BIORAD® AG50W-X8 resin, 200–400 µm mesh size, 1.0 mL resin bed) following the procedure described by Georg et al. (2006) and modified by de Souza et al. (2012). Silicon isotope measurements were performed on the Nu Instruments™ Nu Plasma II MC-ICPMS at GEOMAR equipped with an adjustable source-defining slit set at medium-resolution mode for separation of the ^{30}Si beam from molecular interferences. The Si isotope compositions are reported in the δ-notation, which represents the parts per thousand deviation of the sample ratio from that of the NIST standard NBS28 as follows: $\delta^{30}Si = [(({}^{30}Si/{}^{28}Si)_{sample}/({}^{30}Si/{}^{28}Si)_{NBS28})-1]*1{,}000$. For each sample, the number of analytical replicates (n), individual sessions (S), and chemical preparations (N) is provided in the Supporting Information (Data set S1 in Supporting Information S1). The external reproducibility is reported as 2σ standard deviation (2 SD) of all analytical replicates of the mean $\delta^{30}Si$ value, ranging between 0.12 and 0.33‰ for all samples. The long-term external reproducibility of repeated measurements of the NBS28 standard was within the long-term precision of ±0.20‰ (2 SD), which represents the error bars provided for the majority of the $\delta^{30}Si_{DSi}$ data of our study, except for the few samples with individual 2 SD larger than ±0.20‰ for which the individual 2 SD was used as error bars of the $\delta^{30}Si_{DSi}$ data. All measurements show the expected mass-dependent Si isotope fractionation. For several well-established standard liquid and solid reference materials, a very good agreement with the consensus values of Reynolds et al. (2007) and Grasse et al. (2017) is observed (see Text S1, and Figure S1 in Supporting Information S1).

2.4. Silicon Isotope Fractionation: Closed Versus Open System Model

Rayleigh (closed) and steady-state (open) models can be applied to describe Si isotope fractionation ($^{30}\varepsilon$) during consumption of DSi by diatoms (e.g., de la Rocha et al., 1997; Ehlert et al., 2012). The Rayleigh model assumes a closed system with a single DSi input from external sources, described by $\delta^{30}Si_{DSi} = \delta^{30}Si_{DSi\_0} + {}^{30}\varepsilon \times \ln f$. In contrast, the steady-state model assumes an open system with a continuous supply of nutrients from external sources balanced by continuous removal by diatom productivity (i.e., input = output), which is described by $\delta^{30}Si_{DSi} = \delta^{30}Si_{DSi\_0} + {}^{30}\varepsilon \times (1-f)$. In both equations, $\delta^{30}Si_{DSi}$ corresponds to the measured Si isotope composition of the samples, while $\delta^{30}Si_{DSi\_0}$ represents the corresponding initial or preformed compositions expected from DSi inputs and conservative behavior during mixing. The fraction of remaining [DSi] in solution relative to the initial concentration is described by $f = [DSi]/[DSi]_0$, where [DSi] and $[DSi]_0$ are analogous to $\delta^{30}Si_{DSi}$ and $\delta^{30}Si_{DSi\_0}$. The calculation of $\delta^{30}Si_{DSi\_0}$ and $[DSi]_0$ is provided in Section 2.5. Note that Lena River estuary waters with $\delta^{30}Si_{DSi} < +2‰$ have likely been strongly influenced by DSi redistribution due to sea ice formation and melting and thus are excluded from the calculation of $^{30}\varepsilon$.

2.5. Water Component Analysis, End-Member Values, and Preformed Nutrient and $\delta^{30}Si$ Characteristics

The difference between the observed nutrient concentrations and Si isotope values and the values expected from external inputs and water mass mixing ($[nutrient]_0$ and $\delta^{30}Si_{DSi\_0}$, respectively; hereafter also referred to as *preformed* concentrations and Si isotope compositions) are determined based on the water component analysis of Laukert, Frank, Bauch, Hathorne, Gutjahr et al. (2017). The analysis is based on multiple parameters including salinity, stable oxygen and radiogenic neodymium isotopes, and includes the calculation of the initial salinity corresponding to the salinity expected without the influence of sea ice formation and melting based on oxygen isotope data. This salinity is combined with dissolved neodymium isotope signatures to determine the preformed Nd concentration and the contributions of the major sources (see below) by applying their end-member values (Table 1) and iteratively solving a set of mass balance equations (Laukert, Frank, Bauch, Hathorne, Gutjahr et al., 2017). Salinity and oxygen isotopes are also used to calculate the fractions (f) of river water (f_{RIV}) and sea ice meltwater (f_{SIM}).

Arctic Atlantic Water (AAW), Lena River freshwater (L), and Kara Sea freshwater (KS, essentially Yenisei and Ob River water) are the three major end-members that contribute to the mixture of waters in the Laptev

Table 1
End-Member Compositions of Nutrient Sources Applied in This Study

End-members	Salinity	$\delta^{18}O$	ε_{Nd}	[DIN] (μM)	[DIP] (μM)	[DSi] (μM)	$\delta^{30}Si_{DSi}$ (‰)	$[DSi]_{DIN}$* (μM)	$[DIP]_{DIN}$* (μM)
Arctic Atlantic Water — AAW	34.85[a]	0.2[a]	−9.9 ± 0.34[a]	9.00[a]	0.80[a]	4.89[a]	+1.99 ± 0.28[a]	−4.1[g]	0.24[h]
Kara Sea freshwater — KS	0	−20[b]	−6.0 ± 0.42[c]	1.39[d]	0.09[d]	82.3[e]	+1.6 ± 0.25[e]	80.9[g]	0.00[h]
Lena River summer end-member — L_S	0	−20[b]	−15.7 ± 0.19[c]	1.34[d]	0.11[d]	68[f]	+0.86 ± 0.3[f]	66.7[g]	0.03[h]
Lena River winter end-member — L_W	0	−20[b]	−16.7 ± 0.32[c]	4.43[d]	0.16[d]	141.4[f]	+1.86 ± 0.08[f]	137.0[g]	−0.12[h]

[a]Average of the two samples VB14/17/1/5 and VB13/03/6/190 with typical θ -S characteristics of AAW ($\theta > 0$°C and $S \approx 34.85$) at the Laptev slope (see also Laukert, Frank, Bauch, Hathorne, Gutjahr et al. (2017); Laukert, Frank, Bauch, Hathorne, Rabe et al. (2017)). [b]Values taken from Bauch et al. (2010). [c]Values taken from Laukert, Frank, Bauch, Hathorne, Rabe et al. (2017). [d]Calculated based on seasonal discharge and concentration data from the Arctic Great River Observatory, http://www.arcticgreatrivers.org/data.html. For KS + Ls we calculated averages of the spring freshet periods from 2013 to 2014. For Lw we used winter data from 2011. [e]Values taken from Mavromatis et al. (2016). [f]Values taken from Sun et al. (2018). [g]calculated as $[DSi]_{DIN}* = [DSi] - [DIN]$. [h]calculated as $[DIP]_{DIN}* = [DIP] - ([DIN]/16)$.

Sea (Figure 1). We use the fractions of these end-members calculated by Laukert, Frank, Bauch, Hathorne, Gutjahr et al. (2017) to determine preformed nutrient concentrations and dissolved Si isotope compositions. The end-member values for $\delta^{30}Si_{DSi}$ and [*nutrient*] (Table 1) are well constrained: For AAW, we use the average values of the two samples from approximately 200 m water depth (VB14/17/1/5 and VB13/03/6/190) with typical θ-S characteristics of AAW (Laukert, Frank, Bauch, Hathorne, Gutjahr et al., 2017; Rudels et al., 2012). All nutrient concentrations of our AAW end-member are well in line with literature data and the general circulation scheme of the open Arctic Ocean (see Section 2.2). The corresponding Si isotope composition ($\delta^{30}Si_{DSi} = +1.99 \pm 0.07$‰) is within error identical to the value reported by Varela et al. (2016) for AAW in the Canada Basin ($\delta^{30}Si_{DSi} = +2.04 \pm 0.11$‰). Note that these $\delta^{30}Si_{DSi}$ values are heavier than the value reported for "pristine" Atlantic Water (AW) entering the Arctic Ocean ($\delta^{30}Si_{DSi} \sim +1.5$–$1.7$‰) and "modified" AAW circulating in the central Arctic Ocean ($\delta^{30}Si_{DSi} \sim +1.6$‰) (Debyser et al., 2022; Liguori et al., 2020), likely due to admixture of dense and productive waters from the Barents and Kara Seas to (A)AW at the Laptev Shelf slope (e.g., Laukert, Frank, Hathorne et al., 2017, 2019). End-member values for the Lena River summer and winter $\delta^{30}Si_{DSi}$ are an average of summer signatures (+0.86‰) and the heaviest winter signature (+1.86‰), respectively, and are adapted from Sun et al. (2018), while for the Yenisei River the average summer signature (+1.6‰) is adapted from Mavromatis et al. (2016). The selection of the heaviest winter signature for Lena River winter inputs serves the purpose of identifying relative rather than absolute changes in $\delta^{30}Si_{DSi}$. The value of the Yenisei River is subsequently applied as the KS end-member (Table 1). No $\delta^{30}Si_{DSi}$ data are available for the Ob River but no significant difference is expected between Ob and Yenisei isotope signatures, given that both rivers drain similar lithologies (Pokrovsky et al., 2013). In addition, no significant difference exists between the average [DSi] of these two rivers (~84 μM; calculated based on [DSi] and seasonal discharge data from the Arctic Great River Observatory, http://www.arcticgreatrivers.org/data.html) and the [DSi] reported by Mavromatis et al. (2016) for the Yenisei River (~82 μM). The end-member values for [DIN] and [DIP] are also provided in Table 1 and were calculated in the same way as for [DSi], except that for the Lena River concentrations and seasonal discharge data were also taken from the Arctic Great River Observatory.

The preformed nutrient concentrations are based on the above-described water component analysis and the three end-members and are calculated as $[nutrient]_0 = f_{AAW}*[nutrient]_{AAW} + f_L*[nutrient]_L + f_{KS}*[nutrient]_{KS}$, where *f* and [*nutrient*] are the fractions and the concentrations of the corresponding water component, respectively. The difference btween preformed concentrations to measured concentrations (i.e [*nutrient*]—$[nutrient]_0$) is expressed as Δ[*nutrient*] in percent, with negative and positive numbers reflecting nutrient deficiency and excess, respectively. Zero percent change means that the observed concentrations can be entirely attributed to conservative nutrient behavior resulting from nutrient supply and mixing. Note that the calculation of Δ[*nutrient*] only accounts for net excess or deficiency of nutrient concentrations and does not provide direct information on multiple consecutive nutrient enrichment or depletion phases. We estimate the absolute uncertainty for Δ[*nutrient*] to be 15% for all nutrients based on the accuracy and precision of the nutrient measurements and the uncertainties associated with the water component analysis (Laukert, Frank, Bauch, Hathorne, Gutjahr et al., 2017). The calculation of preformed $\delta^{30}Si_{DSi\_0}$ is performed analogous to that of $[nutrient]_0$ by solving the following equation: $\delta^{30}Si_{DSi\_0} = (f_{AAW}*\delta^{30}Si_{DSi\_AAW}*[DSi]_{AAW} + f_L*\delta^{30}Si_{DSi\_L}*[DSi]_L + f_{KS}*\delta^{30}Si_{DSi\_KS}*[DSi]_{KS})/(f_{AAW}*[DSi]_{AAW} + f_L*[DSi]_L + f_{KS}*[DSi]_{KS})$. The difference between $\delta^{30}Si_{DSi\_0}$ and $\delta^{30}Si_{DSi}$ is reported as $\Delta\delta^{30}Si_{DSi}$ and calculated analogous to Δ[*nutrient*] but instead of percentages it is reported in ‰.

To predict which nutrient becomes limiting for phytoplankton growth, we calculate nutrient concentrations relative to typical phytoplankton requirements (Moore, 2016 and references therein). The distributions of DIP and DSi relative to DIN ([nutrient]$_{DIN}$*) are derived as follows [DIP]$_{DIN}$* = [DIP] − ([DIN]/16) and [DSi]$_{DIN}$* = [DSi] – [DIN]. The end-member values of [DIP]$_{DIN}$* and [DSi]$_{DIN}$* are provided in Table 1. The preformed DIP and DSi distributions relative to DIN ([DIP]$_{DIN}$*$_0$ and [DSi]$_{DIN}$*$_0$, respectively) are calculated identically, except that [*nutrient*]$_0$ is used instead of [*nutrient*]. The differences between [*nutrient*]$_{DIN}$*$_0$ and [*nutrient*]$_{DIN}$* are calculated analogous to Δ[*nutrient*] and reported as Δ[*nutrient*]$_{DIN}$* in μM. [*nutrient*]$_{DIN}$*, [*nutrient*]$_{DIN}$*$_0$, and their difference can only be calculated for the summer samples due to the lack of DIN data from the winter expedition.

3. Results

3.1. Hydrography and Water Mass Distribution

For the investigated years the hydrography and the distribution of the major water mass components (AAW, *L*, KS) have been described elsewhere in detail (Janout et al., 2015, 2017, 2020; Laukert, Frank, Bauch, Hathorne, Gutjahr et al., 2017) and therefore are only briefly summarized here. Sampling in winter 2012 was geographically restricted to a comparatively small area near the Lena River Delta, which was marked by a stratified water column comprising surface waters with near-freezing temperatures and a wide range of salinities (~6–20), and warmer and saltier bottom waters. In contrast, sampling during the summers of 2013 and 2014 was conducted across the entire Laptev Sea. It revealed hydrographic conditions that differed fundamentally between the two years, representing the two extreme hydrographic modes generally observed in the Laptev Sea: Onshore-directed winds in summer 2013 caused spreading of Lena River freshwater throughout much of the eastern and central Laptev Shelf, while strong southerly winds in summer 2014 diverted much of the freshwater to the northeast. This setting resulted in a reduction of f_{RIV} by ~50% and a significantly weaker stratification in the central and southeastern Laptev Sea compared with the previous year (Janout et al., 2020). This shift is also reflected in the surface salinity, which in September 2013 reached only ~5 in the east and ~18 on the central shelf, while in September 2014 it was significantly higher ($S > 20$) (Figure 2). In contrast to the central and southeastern shelf, the northwestern Laptev Sea near Vilkitsky Strait had higher surface salinities in 2013 (S ~28) than in 2014 (S ~22), consistent with a stronger contribution of KS via the Vilkitsky Strait Current as evidenced by higher f_{RIV} and f_{KS} (reaching 20%) above the southern slope of the Vilkitsky Trough in 2014. Surface temperatures on the central shelf in both years reached maximum values at ~4.5°C, while bottom waters had near-freezing temperatures (~−1.8°C). The depth of the seasonal pycnocline was generally shallower in the southeast Laptev Sea and deepened (10–35 m) with distance from the Lena River Delta. Waters below 60 m depth at the Laptev Sea shelf break had salinities above 34 in both years and temperatures ranging between −1.7°C and 1.7°C, with warmest and saltiest ($S = 34.85$) waters forming the core of AAW at ~200 m depth. Sea-ice meltwater (positive f_{SIM}) was encountered in surface waters of the northwestern Laptev Sea during both summers (f_{SIM} up to 11%), while a brine signal (negative f_{SIM}) dominated the central and eastern Laptev Sea (f_{SIM} reaching −12%). Below the pycnocline, variable brine signals dominated the bottom water layer during both summers.

3.2. Nutrient Concentrations, Relationships, and Si Isotope Compositions

In summer, surface nutrient concentrations are generally highest in the southeastern Laptev Sea near the Lena Delta and gradually decrease toward the northern and northwestern Laptev Sea (Figure 2). On average, surface concentrations were higher in 2013 compared to 2014, particularly in the southeastern Laptev Sea, which in 2013 was marked by lower surface salinities reflecting a larger f_L (Figure 2). Each nutrient exhibits a unique water column distribution that was similar in both summers and was marked by highly variable concentrations on the shelf (<~60 m depth) but essentially constant concentrations above the shelf slope (>~60 m depth) (Figure 3). Summer [DSi] ranged between 0.44 and 54.9 μM and is only weakly correlated with salinity ($R^2 = 0.31$) but moderately correlated with f_L ($R^2 = 0.69$). Summer [DSi] is not correlated with [DIN] or [DIP] and both nutrients are only weakly correlated with one another ($R^2 = 0.42$). For samples with river fractions >10%, however [DSi] is weakly correlated with [DIP] ($R^2 = 0.27$) and moderately correlated with [DIN] ($R^2 = 0.51$). Summer [DIN] and [DIP] range from zero to 11.6 μM and from 0.08 to 1.4 μM, respectively, while winter nutrient concentrations are significantly higher with [DSi] and [DIP] reaching 136.5 μM (isotope sample with lowest surface salinity and highest f_L) and 4.7 μM (bottom layer sample with high salinity), respectively.

The summer distributions of DIP and DSi relative to DIN ([DSi]$_{DIN}$* and [DIP]$_{DIN}$*) range between −0.1 and 0.9 μM and between −5.9 and 52 μM, respectively (Figure 4). [DIP]$_{DIN}$* are highest in bottom water samples with

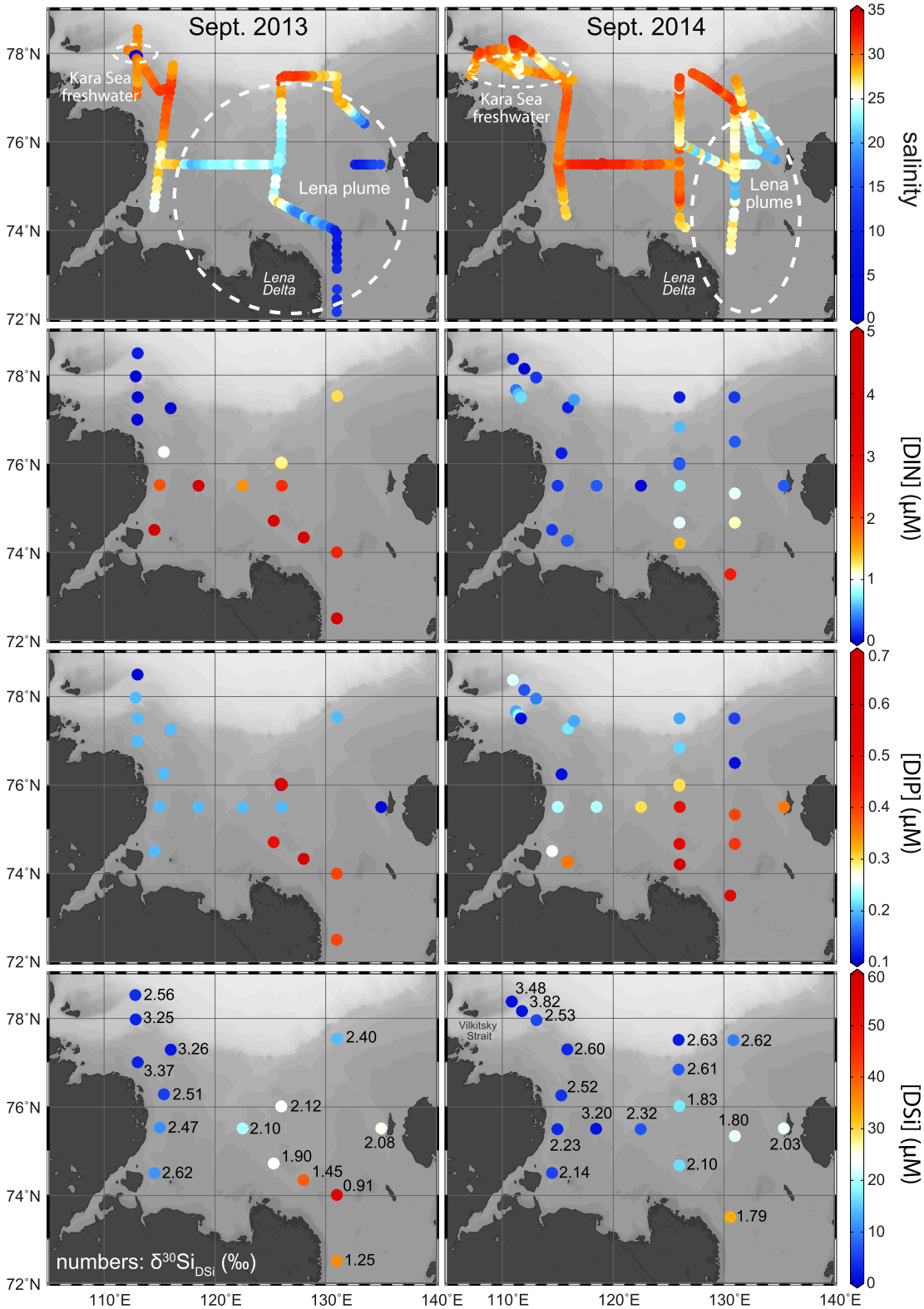

Figure 2. Surface distribution of salinity (Janout et al., 2015, 2020), dissolved inorganic nitrogen ([DIN]), dissolved inorganic phosphorus ([DIP]), and silicic acid concentrations ([DSi]) for the summers of 2013 and 2014. Silicon isotope signatures ($\delta^{30}Si_{DSi}$) are reported as numbers next to the color coded [DSi].

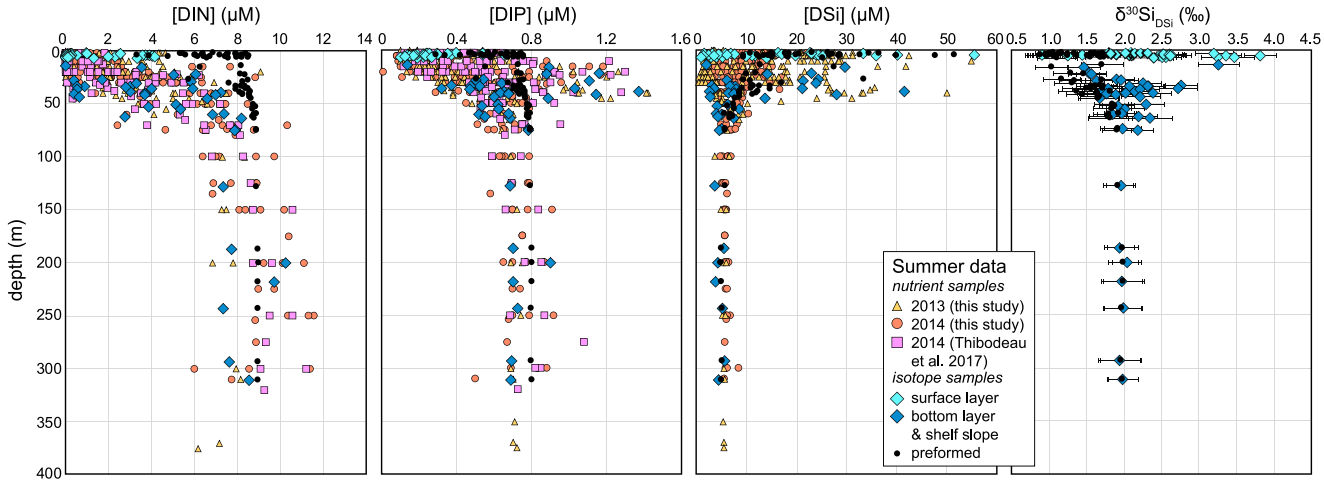

Figure 3. Dissolved inorganic nitrogen ([DIN]), dissolved inorganic phosphorus ([DIP]), and silicic acid ([DSi]) concentrations as well as dissolved stable silicon isotopes ($\delta^{30}Si_{DSi}$) plotted against depth. Error bars for $\delta^{30}Si_{DSi}$ represent the long-term precision of ±0.20‰ (2σ) or individual sample error in case it is higher. Note that [DIN] and [DIP] for the isotope samples were interpolated from concentrations obtained from the nutrient samples, while [DSi] was determined in the isotope samples. Estimated preformed [*nutrient*] and $\delta^{30}Si_{DSi}$ values are shown in addition and correspond to the concentrations and isotope signatures expected from external inputs and conservative behavior based on a previously developed water component analysis (Laukert, Frank, Bauch, Hathorne, Gutjahr et al., 2017).

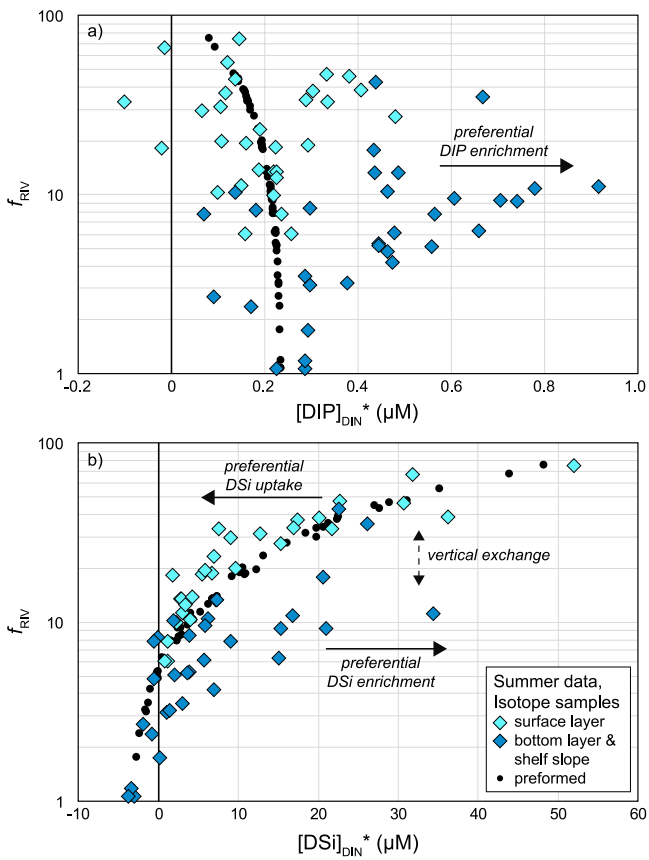

Figure 4. (a) $[DIP]_{DIN}^*$ ($[DIP] - ([DIN]/16)$) and (b) $[DSi]_{DIN}^*$ ($[DSi] - [DIN]$) plotted against the river fraction f_{RIV} calculated based on salinity and oxygen isotopes. For better data illustration, a logarithmic scale is used for f_{RIV}. For interpretation of the trends, see Section 3.2.

f_{RIV} ~10%, whereas lowest $[DIP]_{DIN}^*$ are calculated for the surface samples, which on average have a $[DIP]_{DIN}^*$ value of 0.2 µM. In contrast $[DSi]_{DIN}^*$ are highest in surface samples with the highest f_{RIV} in the southeastern Laptev Sea, whereas lowest $[DSi]_{DIN}^*$ are determined for bottom water and shelf slope samples in the northeastern Laptev Sea. $[DIP]_{DIN}^*$ correlates with f_{RIV} neither in the surface nor in the bottom layer ($R^2 < 0.2$), while $[DSi]_{DIN}^*$ decreases in both layers with decreasing f_{RIV} ($R^2 = 0.86$ and 0.53 for surface and bottom water samples, respectively) reaching 0.8 µM in the surface layer (station 2, 2014). Highest $[DSi]_{DIN}^*$ values in the bottom layer (up to 34 µM) are calculated for the samples with the highest $[DIP]_{DIN}^*$.

The $\delta^{30}Si_{DSi}$ signatures are similar for both summers ranging between +0.91 and +3.82‰. Lowest $\delta^{30}Si_{DSi}$ values are observed in surface waters near the Lena River Delta and highest values are confined to surface waters of the northern and northwestern Laptev Sea (Figure 2). $\delta^{30}Si_{DSi}$ variability decreases with water depth reaching constant signatures around +2‰ at the Laptev Shelf slope (>60 m depth) (Figure 3). The surface $\delta^{30}Si_{DSi}$ signatures are negatively correlated with [DSi] obtained from the isotope samples ($R^2 = 0.72$, Figure 5a) and positively with initial salinity S_0 ($R^2 = 0.69$), while no strong correlations are observed below the pycnocline. $\delta^{30}Si_{DSi}$ and [DSi] measured in winter samples collected near the Lena Delta deviate strongly from the summer distribution, with a high range in [DSi] (33–136.5 µM) and less variable $\delta^{30}Si_{DSi}$ values ranging between +1.48‰ and +1.74‰. In winter, the highest $\delta^{30}Si_{DSi}$ (+1.74‰) was associated with the highest [DSi] (136.5 µM).

3.3. Deviations From Preformed Nutrient Concentrations and $\delta^{30}Si_{DSi}$ Compositions

Large differences exist between the observed and preformed summer concentrations (Δ[*nutrient*]) (Figures 3 and 6). Apart from two samples with highest f_L (stations 19 and 20 from 2013), surface samples are marked by pronounced DIN loss (Δ[DIN] < −35%), which increases from the southeastern toward the northwestern Laptev Sea until complete DIN removal is

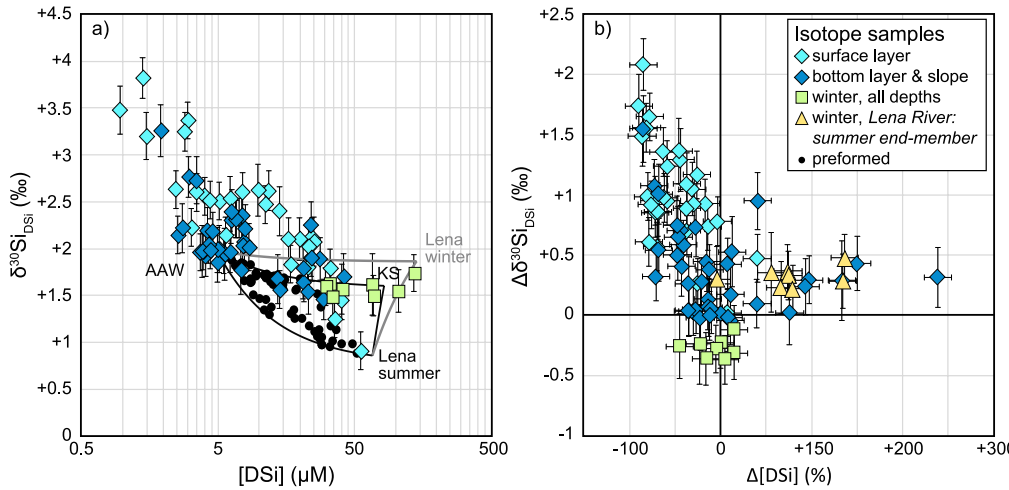

Figure 5. (a) Three end-member mixing diagrams showing the dissolved stable Si isotopes ($\delta^{30}Si_{DSi}$) plotted against silicic acid concentrations ([DSi]). In general, the summer end-member values were used, except for the winter samples for which primarily the winter end-member of the Lena River was applied. Samples that do not fall in the mixing triangle are clearly influenced by nonconservative processes (e.g., uptake and loss of DSi). (b) Change of preformed to measured Si isotope and DSi concentrations ($\Delta\delta^{30}Si_{DSi}$ in ‰ and Δ[DSi] in %, respectively). For interpretation of these figures, see Section 4.1.1.

reached (Δ[DIN] = −100%). The distributions of DIP and DSi loss are similar, except that complete removal is not achieved (Δ[DIP] and Δ[DSi] only reach −86% and −90%, respectively). Pronounced but overall smaller loss of all nutrients is also observed in bottom water samples recovered in the northwestern Laptev Sea (Δ[DIN], Δ[DIP], and Δ[DSi] reach −95%, −57%, and −85%, respectively). In contrast, bottom water samples recovered in the southeastern Laptev Sea beneath the Lena River plume are marked by strong DIP and DSi excesses (Δ[DIP] and Δ[DSi] reach +89% and +240%, respectively). Weak local DSi enrichment is also observed in the northwestern Laptev Sea (Δ[DSi] ∼ +10%). Above the Laptev Shelf slope at depths >60 m, no significant changes between measured/interpolated and preformed concentrations are observed and the Δ[*nutrient*] values scatter around zero % (Figures 6a–6c).

A moderate correlation between Δ[DSi] and f_{RIV} exists for the surface samples ($R^2 = 0.63$) but samples with f_{RIV} ∼40% deviate toward weaker DSi loss (Figure 6f), a trend that is also observed for the loss distributions of DIN and DIP (Figures 6d and 6e). Samples with DIP and DSi excess beneath the Lena River plume also have elevated f_{RIV} (up to ∼10%) and negative f_{SIM}. Positive f_{SIM} are only present in some of the surface samples (Figures 6g–6i). Δ[DSi] of the winter samples varies between +15 and −45% when the winter end-member is applied for the Lena River.

Differences also exist between the observed and preformed DIP and DSi distributions relative to DIN (see difference between observed and preformed values in Figure 4). Highest $\Delta[DIP]_{DIN}$* values are determined for the bottom water samples reaching 0.7 µM in 2013 at station 17. In contrast, the lowest $\Delta[DIP]_{DIN}$* values are calculated for the surface samples reaching −0.3 µM in 2013 at station 9. The trend in $[DIP]_{DIN}$* (decrease with decreasing f_{RIV}) is mirrored in $[DSi]_{DIN}*_{\_0}$ but marked deviations from the preformed deficiency distribution exist for the surface and the bottom layer. Essentially all surface samples have negative $\Delta[DSi]_{DIN}$* reaching −14.3 µM in the sample with the lowest $\Delta[DIP]_{DIN}$*. In contrast, almost all shelf bottom water samples have positive $\Delta[DSi]_{DIN}$* values reaching 30.2 µM in the sample with the highest $\Delta[DIP]_{DIN}$*.

The difference between $\delta^{30}Si_{DSi\_0}$ and $\delta^{30}Si_{DSi}$ ($\Delta\delta^{30}Si_{DSi}$) for the summer samples ranges between 0 and +2‰ (Figure 5b). Samples with the lowest Δ[DSi] have the highest $\Delta\delta^{30}Si_{DSi}$, meaning that DSi loss is accompanied by a shift toward heavier $\delta^{30}Si_{DSi}$ values. Summer bottom samples with marked DSi excess have $\Delta\delta^{30}Si_{DSi}$ ranging between 0 and +0.5‰. This range in $\Delta\delta^{30}Si_{DSi}$ also applies to the winter samples, provided that the summer end-member for the Lena River is used. The winter samples have $\Delta\delta^{30}Si_{DSi}$ around −0.25‰ at Δ[DSi] scattering between 0% and −50% when the winter end-member is applied for the Lena River.

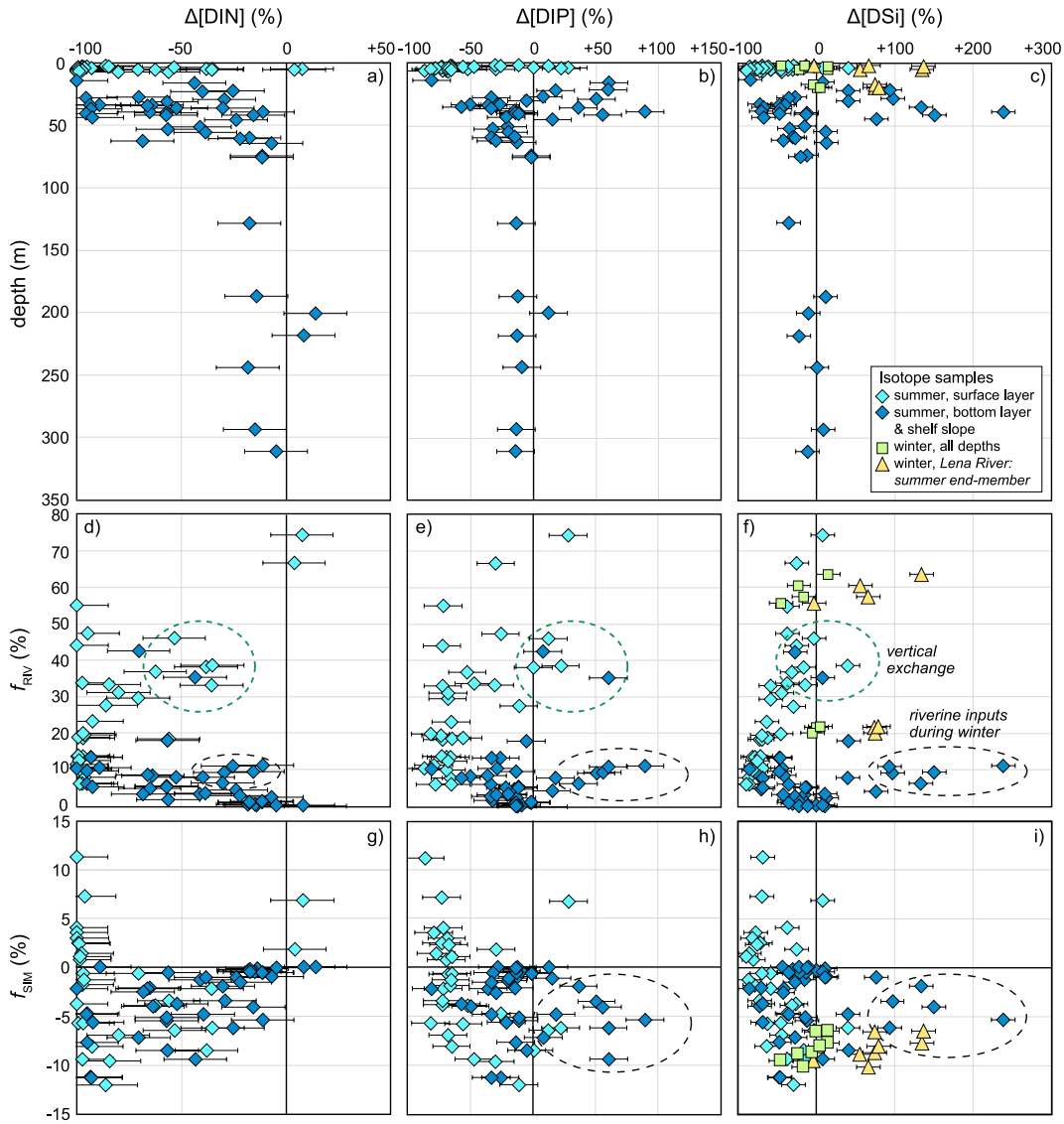

Figure 6. Change of preformed to observed nutrient concentrations (Δ[*nutrient*], in percent) plotted against depth (a–c), the river water fraction f_{RIV} (d–f), and the fraction of sea ice meltwater f_{SIM} (g–i). Note that one winter sample has $f_{RIV} > 80\%$ and thus plots outside the visible range in the Δ[DSi] plots (c, f, i). Samples with Δ[*nutrient*] > 0% are marked by nutrient excess, while samples with Δ[*nutrient*] < 0% exhibit nutrient deficiency compared to what can be expected from external nutrient inputs and conservative behavior (i.e., Δ[*nutrient*] = 0%). The absolute uncertainty for Δ[*nutrient*] is estimated at 15% for all nutrient changes (see Section 2.5 for more information).

4. Discussion

4.1. Mechanisms Controlling Nutrient Distributions in the Laptev Sea

4.1.1. Marine and Riverine Inputs Versus Biological Uptake in Surface Waters

The summer distributions of macronutrients in the surface layer of the Laptev Sea reflect the interplay between marine (AAW) and riverine (L, KS) inputs and utilization by phytoplankton. Highest nutrient concentrations were encountered in the southeastern Laptev Sea in surface waters with lowest salinities and highest f_{RIV} (Figure 2, in 2013 reaching 4.7, 1.1, and 55.6 µmol/kg for [DIN], [DIP], and [DSi], respectively). These waters are marked by weaker or no nutrient loss (Δ[*nutrient*] ≈ 0%, Figure 6), suggesting conservative behavior and hence a dominant role of the contributing water masses and their mixing (*L* for DSi and AAW for DIN and DIP) in generating these high concentrations. Nutrient supply through erosion of coastal soils (Terhaar et al., 2021 and references therein) does not seem to have a major effect on the nutrient distributions as this would be likely reflected in markedly

higher Δ[*nutrient*], given that our analysis does not account for such additional inputs. The dominance of the Lena River in supplying most of the DSi is further supported by low $\delta^{30}Si_{DSi}$ values near the Lena River Delta (in 2013 reaching +0.91‰ at station 19, Figure 2) approaching those of the summer Lena River end-member ($\delta^{30}Si_{DSi}$ = +0.86‰, Sun et al., 2018). Contributions of DIN and DIP through coastal erosion cannot be entirely excluded but will likely achieve a similar magnitude as the riverine inputs (Terhaar et al., 2021), which will be significantly smaller than inputs via advection of DIN- and DIP-rich AAW (Table 1). Highest surface Δ[DIN] around zero percent were calculated for the two samples with highest f_{RIV} (>60%) recovered near the Lena River Delta (stations 19 and 20, 2013, see also Figure 6), which in the case of DIN argues against major additions through external sources other than those identified in our study.

Progressing nutrient utilization by phytoplankton toward the northern and northwestern Laptev Sea is evident from decreasing nutrient concentrations and increasing nutrient loss (i.e., Δ[*nutrient*] becomes more negative). This distribution suggests that the presence of Lena River freshwater has a profound effect on biological uptake, given that moderate correlations are observed for DIN ($R^2 = 0.50$), DIP ($R^2 = 0.42$), and DSi ($R^2 = 0.63$) between Δ[*nutrient*] and f_{RIV} in the surface layer (Figures 6d–6f). For the northern Laptev Sea, our Si isotope fractionation model indicates closed system DSi uptake (see further below), consistent with a strong single DSi input during the spring freshet and no significant additions during the summer months when the Lena River discharge is low (Holmes et al., 2012). In contrast, there is little to no DSi loss in the southeastern Laptev Sea despite the highest productivity rates in the months prior to sampling. There, low DSi loss can either be attributed to the rapid and continuous influx of riverine nutrients during the summer months and/or to the influence of riverine freshwater and its constituents on light availability. Light-absorbing substances, such as colored dissolved organic matter, have high concentrations in the river plume (Heim et al., 2014; Hölemann et al., 2021) and limit the depth of the photic zone (Soppa et al., 2019). These substances may have suppressed nutrient utilization at high f_{RIV} (>60%) and in addition to a continuous supply of river-borne nutrients during the summer months, helped maintain high nutrient concentrations below and possibly above the pycnocline (Demidov et al., 2021).

Scatter in the loss distributions of DIN and DIP in the Δ[*nutrient*]-f_{RIV} space mainly results from weaker losses at f_{RIV} = 30–40% compared to what can be expected from continuous utilization of river-borne nutrients (Figures 6d–6f). The corresponding surface samples were mainly recovered north of the Lena River Delta and had negative f_{SIM} suggesting admixture of brine- and nutrient-rich waters (Figures 6g–6i, Section 4.1.2). Two bottom water samples collected below the pycnocline (station 13, 2013; station 18, 2014) have f_{RIV}, f_{SIM}, and Δ[*nutrient*] similar to these surface samples, which supports vertical exchange between the bottom waters and the surface mixed layer in this region. The strong stratification in the southeastern Laptev Sea generally dampens the effect of vertical mixing during the summer months (Bauch et al., 2012; Janout et al., 2020). However, multiple storms occurred shortly before and during the sampling campaigns in late September and may have temporarily and locally weakened stratification (e.g., Kassens & Volkmann-Lark, 2013), likely enabling limited vertical exchange and upward supply of nutrient- and brine-rich bottom waters before pycnocline reestablishment. We therefore suggest that local storm-induced stratification breakdowns in late summer are responsible for stimulating primary productivity at f_{RIV} <50% and thus far later than initial estuarine stimulation through direct nutrient inputs via the Lena River (Heiskanen & Keck, 1996).

Outside of the direct influence of the Lena plume, DIN additions to the photic layer must also have contributed to the strong drawdowns observed for DIP and DSi in the northwestern Laptev Sea, given that such drawdowns cannot be explained by biological utilization of riverine DIN only (see also Le Fouest et al., 2013). DIN inputs to the surface layer likely occur through admixture of DIN-rich (~9 μM) AAW (Bauch & Cherniavskaia, 2018), whose contribution to the entire water column of the Laptev Sea is not only indicated by high [DIN] (reaching ~9 μmol/kg in the bottom layer) but also evidenced by high AAW fractions (reaching 90%) determined for the surface layer in this region. DIN addition from the deep marine pool to the surface layer is consistent with previous nutrient budget assessments (Nitishinsky et al., 2007) and likely attributable to wind- and storm-induced mixing and deepening of the pycnocline in late fall and early winter (Hölemann et al., 2011; Janout et al., 2016, 2020). The seasonal erosion of stratification homogenizes nutrient concentrations in the entire water column but has no effect on Δ[DIN], which therefore only reflects nutrient utilization. The photic zone outside the Lena plume can extend to a depth of 30 m (Demidov et al., 2014; Mosharov, 2010; Sorokin & Sorokin, 1996), which is consistent with low [DIN] and elevated DIN loss due to nutrient utilization observed in the upper 20–30 m of the water column during both summers. However, strong nutrient loss is also observed below the photic zone (Δ[DIN] reaches −95% in bottom waters of the southwestern Laptev Sea). This loss likely results from homogenization of

the depleted summer water column during downward progression of the pycnocline, a process that occurs only outside the river plumes and is therefore largely confined to the northern Kara Sea and the northwestern Laptev Sea. This suggests that preformed nutrient levels, as expected from conservative behavior (i.e., external inputs and water mass mixing), particularly in the northwestern Laptev Sea, are unlikely to be reached due to strong utilization. Denitrification in the water column may also lead to pronounced DIN loss but is not expected to occur in the water column of the well-oxygenated Laptev Sea (Thibodeau et al., 2017). The exact impact of sedimentary denitrification (e.g., Sun et al., 2021; Tanaka et al., 2004) on the DIN distribution in the entire Laptev Sea remains to be investigated in dedicated process studies.

DIN is considered the limiting nutrient for primary producers in the Siberian Interior Shelf Seas including the Laptev Sea (Dittmar & Kattner, 2003; Kattner et al., 1999; Nitishinsky et al., 2007; Pivovarov et al., 2005; Reyes & Lougheed, 2018; Thibodeau et al., 2017), consistent with complete DIN utilization ($\Delta[DIN] = -100\%$) in the photic layer observed at a few stations in the northwestern Laptev Sea in 2013 and multiple stations in 2014 in the northern and central Laptev Sea (Figures 2, 3, and 6a). The loss distributions of DIP and DSi mirror that of DIN during both summers, with strongest drawdowns (Δ[DIP] and Δ[DSi] both reach up to $\sim -90\%$) observed in DIN-limited regions where [DIP] and [DSi] reach 0.1 and 0.4 µmol/kg, respectively (Figures 2, 3, 6b, and 6c). However, despite widespread DIN limitation the demand of DSi may be higher for diatoms than that of DIN, as can be inferred from $[DSi]_{DIN}^*$, a parameter used to relate DSi to DIN uptake and hence to derive DSi deficiency relative to that of DIN (Moore, 2016 and references therein). In presence of adequate light and nutrient availability, diatoms generally incorporate Si and N in a molar ratio of 1:1, which results in $[DSi]_{DIN}^* \geq 0$ (Brzezinski, 1985; Ragueneau et al., 2000). In the surface waters of the Laptev Sea $[DSi]_{DIN}^*$ decreases from the southeastern to the northwestern Laptev Sea, where $[DSi]_{DIN}^*$ reaches values as low as ~0.8 µmol/kg (Figure 4b; Figure S2 in Supporting Information S1). This decrease partly reflects mixing between the riverine freshwater and AAW, given that the river end-members have much higher $[DSi]_{DIN}^*$ (>~65 µmol/kg) compared to AAW (~−4.1 µmol/kg). However, by applying our water component analysis, we can eliminate the effect of source inputs and mixing. This allows us to determine negative $\Delta[DSi]_{DIN}^*$ (reaching −14.3 µM) for essentially all surface samples, indicating preferential DSi utilization in the surface layer of the Laptev Sea (see discussion below). Only a few surface samples with f_{RIV} ~40% are marked by higher $[DSi]_{DIN}^*$ than expected from source inputs and mixing, providing further evidence of the admixture of DSi- and DIP-enriched bottom waters to these surface waters due to vertical mixing. To decrease the additional DSi supplied via admixture of AAW, even stronger preferential DSi utilization would be required than what can be inferred from the difference between preformed and actual $[DSi]_{DIN}^*$. In contrast to DSi, DIP is mainly available in excess compared to DIN, which is indicated by most bottom samples being marked by positive $[DIP]_{DIN}^*$ and $\Delta[DIP]_{DIN}^*$ reaching 0.7 µM (Figure 4a).

Deviations from the classical Redfield ratios have been reported for other shallow shelf regions of the Arctic Ocean, for example, for the Beaufort and the Chukchi Seas, where nutrient drawdown is characterized by lower DIN:DIP and higher DSi:DIN ratios (Tremblay et al., 2015). While our calculations indicate that the preferential enrichment of DIP compared to DIN (positive $\Delta[DIP]_{DIN}^*$) cannot be explained by a lower DIN:DIP drawdown ratio (e.g., 13 instead of 16), a higher DSi:DIN ratio (e.g., 2 instead of 1) could account for the negative $\Delta[DSi]_{DIN}^*$ values of the surface samples, suggesting higher consumption of DSi relative to DIN in the surface layer of the Laptev Sea. Preferential DSi uptake can be ascribed to iron limitation, species-specific differences in optimal DSi requirements, DIN limitation, or low irradiance (Tremblay et al., 2008 and references therein). The high riverine input of dissolved iron by the Lena River (Blunden & Arndt, 2019) argues against iron limitation in the Lena River estuary, even though most of it must be removed on the shelves through scavenging and flocculation (Charette et al., 2020). Iron deficiency has been suggested for AW entering the Arctic Ocean through Fram Strait (Krisch et al., 2020) and AAW advected via the Arctic Ocean Boundary Current along the Siberian Shelf margin (Klunder et al., 2012; Rijkenberg et al., 2018). The advection and admixture of iron-depleted AAW to the northwestern Laptev Sea may thus be a reasonable explanation for the higher utilization of DSi relative to DIN in this region. Krisch et al. (2020) recently reported that in the AW-dominated surface waters of eastern Fram Strait (precursor to the AAW), limitation of DSi is approached along with limitation of DIN and iron, which is consistent with the very low surface [DSi] value in the AAW-dominated northwestern Laptev Sea.

The assumption that diatoms play an important role in the utilization and cycling of Si and the other two macronutrients is confirmed by evaluation of dissolved stable Si isotope compositions. For the late summer data, the utilization of the macronutrients is accompanied by a shift toward heavier $\delta^{30}Si_{DSi}$ reaching ~+3.8‰ in the northwestern Laptev Sea (Figure 2), which we ascribe to nutrient uptake by diatoms in agreement with diatom-dominated productivity in the Laptev Sea (Cremer, 1999; Fahl et al., 2001; Tuschling, 2000). In $\delta^{30}Si_{DSi}$-[DSi] space, DSi

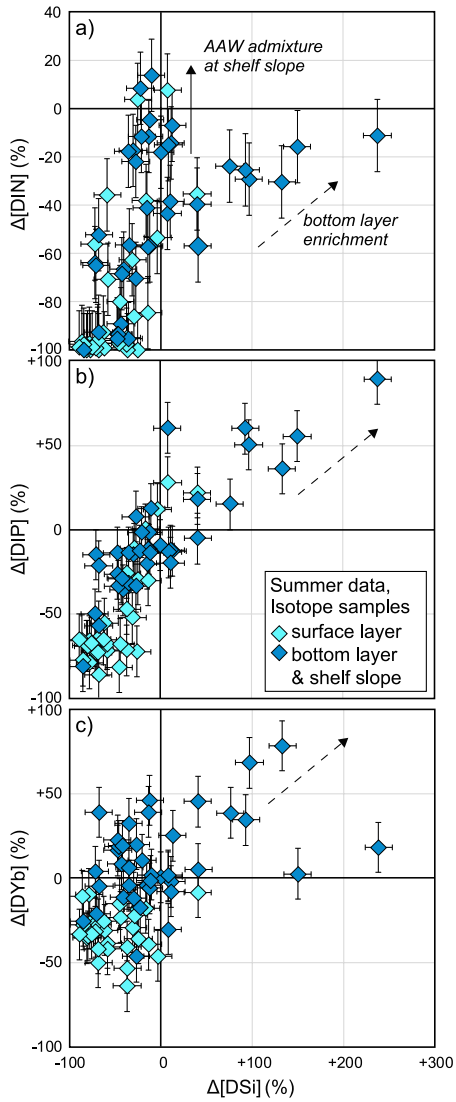

Figure 7. Preformed to observed changes in (a) dissolved inorganic nitrogen (Δ[DIN]), (b) dissolved inorganic phosphorus (Δ[DIP]), and (c) dissolved ytterbium (Δ[DYb]) concentrations plotted against the change in silicic acid concentration (Δ[DSi]). For interpretation of the trends, see Section 4.1.2.

uptake by diatoms for most samples results in compositions plotting outside of the mixing envelope defined by the three end-members through higher $\delta^{30}Si_{DSi}$ signatures and lower [DSi] values (Figure 5a). This process is also reflected in the $\Delta\delta^{30}Si_{DSi}$-Δ[DSi] space (Figure 5b), which relates nonconservative changes in $\delta^{30}Si$ to those observed in [DSi]. Modeling the Si isotope fractionation indicates that both Rayleigh-type (closed) and steady-state (open) conditions could account for the summer $\delta^{30}Si_{DSi}$ distribution in the southeastern Laptev Sea. However, only the steady state would be consistent with a continuous influx of riverine nutrients during the summer months (see discussion above). In contrast, in the northern Laptev Sea, where the fraction of remaining [DSi] in solution relative to the initial concentration falls below ~0.2, the Rayleigh-type model would best explain the $\delta^{30}Si_{DSi}$ distribution in support of a long-distance advection of the single DSi input from the annual spring freshet of the Lena River (Figure S3 in Supporting Information S1). The fractionation factor ($^{30}\varepsilon$) for the entire surface layer of the Laptev Sea for the Rayleigh model is −1.34‰ (±0.87‰, 1SD), while that of the steady-state (open system) model is −2.04‰ (±0.88‰, 1SD). Considering the large uncertainties arising from the differing end-member compositions (*L* and AAW), both fractionation factors agree well with laboratory estimates, although the steady-state value is at the upper end of the compositional range reported in the literature to date (de la Rocha et al., 1997; Meyerink et al., 2017; Milligan et al., 2004; Sun et al., 2014; Sutton et al., 2013, 2018). Sun et al. (2018) also observed a small increase in $\delta^{30}Si_{DSi}$ of the Lena River from spring to summer, which could be superimposed on the Laptev Sea signal but is hardly distinguishable. Field-based estimates in the Beaufort Sea and the Canada Basin vary between −0.33 (closed system) and −1.28‰ (open system) (Giesbrecht et al., 2022; Varela et al., 2016). The latter point to an open system model for the Canada Basin but as the authors of both studies pointed out, the seasonal near quantitative drawdown of DSi occurring in this region would be more consistent with a closed system model. Varela et al. (2016) therefore invoked seasonal DSi drawdown occurring in sea ice to explain the discrepancy between observed and expected $^{30}\varepsilon$ in the Canada Basin. In contrast, the Laptev Sea was essentially ice-free during the sampling campaigns in September 2013 and 2014 and pelagic diatoms rather than sea ice diatoms processed all DSi, which can be inferred from the absence of the latter in preceding years with similar conditions (Polyakova et al., 2021).

A shift toward heavier $\delta^{30}Si_{DSi}$ at increasing/high utilization as observed for the late summer data sets cannot be identified for the winter samples. Instead, all samples are marked by slightly lighter $\delta^{30}Si_{DSi}$ than expected from conservative mixing ($\Delta\delta^{30}Si_{DSi} = -0.25‰$) when the winter Lena River end-member is applied (Figure 5b). This shift is within analytical error (±0.2‰) but appears to be systematic and may result from strong interannual variability in the composition of the Lena River end-member (Sun et al., 2018), which we cannot account for in our assessment of nutrient and $\delta^{30}Si_{DSi}$ distributions. Lena River end-member variability could also explain the wintertime decrease in [DSi] (Δ[DSi] reaches up to −50%), given that [DSi] of the Lena River winter end-member is known to vary strongly between years (Sun et al., 2018).

4.1.2. Bottom Layer Enrichment: Sea Ice-Driven Accumulation and Remineralization

We observed strong enrichments of DSi and DIP (Δ[DSi] and Δ[DIP] reach +240% and +90%, respectively) in the bottom layer of the southeastern Laptev Sea during both summer campaigns (Figure 6). All bottom water samples have a high AAW fraction but samples with the highest DSi and DIP excess were recovered beneath the Lena River plume and had an elevated f_R (up to 10%) and negative f_{SIM} (up to −10%) (Figures 6d–6f and 6g–6i, respectively), indicating combined contributions of riverine freshwater and sea ice-derived brines. As shown in Figure 7, these excesses are positively correlated with one another and with changes observed in [DIN] despite all samples being marked by DIN loss. A correlation with excess DSi is also found for ytterbium (Yb), a heavy

REE whose dissolved distribution in the Laptev Sea is controlled by sea ice formation and melting in addition to riverine inputs, mixing, and limited estuarine removal (Laukert, Frank, Bauch, Hathorne, Gutjahr et al., 2017). The simultaneous accumulation of bio-essential nutrients and essentially bio-inactive trace elements (e.g., Yb) at increasing f_{RIV} and decreasing f_{SIM} suggests the admixture of river- and brine-rich waters to be the primary driving mechanism of nutrient enrichments rather than biogeochemical or biological processes.

Previous investigations attributed DIP and DSi enrichments in bottom waters exclusively to in situ nutrient remineralization from the decomposition of organic matter (Cauwet & Sidorov, 1996; Codispoti & Richards, 1968; Létolle et al., 1993; Nitishinsky et al., 2007). Apart from the lack of direct evidence of this process for the bottom layer beneath the Lena River plume, the findings of Codispoti and Richards (1968) cast doubt on nutrient enrichment by a single process, given that some of their bottom water samples in the Lena estuary had [DSi] exceeding the maximum amount attributable to phytoplankton decomposition. All of our winter samples recovered near the Lena River Delta in 2012 have also high [DSi] and [DIP] and a Δ[DSi] near zero percent when the winter end-member is used for the Lena River, suggesting a riverine origin of these nutrients during winter. However, these winter samples exhibit an apparent DSi excess of up to +140% when the summer end-member for the Lena River is used (Figures 6c, 6f and 6i). This end-member adjustment allows to evaluate the role of riverine winter inputs to the summer nutrient distribution. The resulting apparent excess is similar to that determined for most bottom water samples recovered during the late summer campaigns in 2013 and 2014 and thus consistent with preservation of winter water and nutrients in the bottom layer during summer (Bauch et al., 2009, 2010; Nitishinsky et al., 2007). Thibodeau et al. (2017) identified a strong atmospheric contribution of nitrogen to the bottom layer, which they attributed to winter convective mixing and injection of brine-enriched dense waters resulting from sea ice formation into the bottom layer. Hölemann et al. (2021) also concluded that the distribution of dissolved organic matter in the Laptev Sea water column is strongly influenced by the formation and melting of sea ice. Sea ice formation is accompanied by rejection of a high proportion of nutrients and other seawater constituents into the underlying water (Meiners & Michel, 2016), resulting in highly enriched brines that can sink to the bottom layer due to their high density (Bauch et al., 2009, 2010). They could enable transport of nutrient-rich dense waters with elevated f_{RIV} to the bottom layer and thus explain the nutrient excess beneath the Lena River plume. Due to the thin photic layer (~5 m) of the Lena River plume (Soppa et al., 2019) and the relatively long residence time (at least one seasonal cycle) of bottom waters in the Laptev Sea (Bauch et al., 2009), these nutrient enrichments are preserved throughout the year.

The residence time of the Lena River plume is not precisely known for the Laptev Sea but is likely to range from a few months to slightly more than a year, depending on prevailing wind conditions (cf. Janout et al., 2020). Therefore, redistribution of nutrients in winter by sea ice formation could also affect nutrients supplied through the Lena River in spring and summer that have not been utilized by phytoplankton during the productive season. This is supported by the elevated nutrient levels in the Lena River plume in late September (Δ[nutrient] reaching 0%, see Section 4.1.1) and thus shortly before the onset of sea ice formation in October. To quantify the contribution of summer and winter DSi inputs from the Lena River, the primary DSi source in the Laptev Sea, to the excess beneath the Lena River plume, we calculated the summer and winter flow-weighed DSi inputs and compared them to the inventory of excess DSi in the bottom layer beneath the Lena River plume. We estimated the excess DSi to be 10 μM and the volume of the area with accumulated nutrients to be 1,250 km^3, corresponding to a water body of 250*250*0.02 km. Nutrient input from the Lena River is lower in winter than in summer due to lower discharge and despite higher concentrations. Nevertheless, depending on the values chosen for Lena River discharge (R-ArcticNET or Whitefield et al. (2015)) and [DSi] (Arctic Great River Observatory or Sun et al. (2018)), the winter DSi contribution is 327–680*10^9 g and corresponds to 17%–49% of the Lena River inputs in spring and summer, which is estimated to be 1387–1981*10^9 g. Fluxes reported by Holmes et al. (2012) for the different seasons and by Le Fouest et al. (2013) and the references therein for the whole year are somewhat lower than those reported here (the maximum annual DSi flux reaches only 1640*10^9 g), but the proportion between winter and summer fluxes determined by Holmes et al. (2012) is within the range. The winter contribution of the Lena River flux accounts for 44%–90% of the accumulation in the bottom layer (751*10^9 g), while spring and summer inputs could contribute 185%–264% if no biological uptake occurred. Although this is only a rough estimate due to the high uncertainties in the end-members, it demonstrates that the winter DSi input from the Lena River, combined with a small portion of the summer DSi input, could indeed account for the DSi enrichment under the Lena plume.

Si isotopes further support our hypothesis that DSi enrichment in the bottom layer is mainly established during winter via sea ice formation. The $\delta^{30}Si_{DSi}$ signatures of the summer bottom waters with high DSi excess recovered beneath the Lena plume range between +1.5‰ and +1.9‰ and thus are within error identical with the

Si isotope signatures determined for the winter samples ($\delta^{30}Si_{DSi}$ between +1.5‰ and +1.7‰). Moreover, the difference between $\delta^{30}Si_{DSi}$ and $\delta^{30}Si_{DSi\_0}$ for both winter and summer waters is low ($\Delta\delta^{30}Si_{DSi}$ only reaches ~0.5‰), which is in line with the wintertime origin of these waters and no substantial consumption of bottom water nutrients during summer. DSi additions to the bottom waters resulting from the dissolution of biogenic Si from settled diatom frustules would likely imprint lighter $\delta^{30}Si_{DSi}$ signatures, given that diatoms formed in the Lena River plume likely have very light $\delta^{30}Si_{diatom}$ compositions around +0.6‰ based on a $^{30}\varepsilon$ of −1.34‰ (Section 4.1.1) and the $\delta^{30}Si_{DSi}$ of surface waters in this region (average $\delta^{30}Si_{DSi}$ = +2‰, 2 SD = 0.3, n = 6). In contrast, outside the Lena River plume in the northwestern Laptev Sea, elevated [DSi] and low DSi excess reaching ~10% in bottom waters (50 m depth, stations 7 and 6 from 2013 to 2014, respectively) are consistent with in situ diatom dissolution, given that the expected $\delta^{30}Si_{diatom}$ signatures of settling diatoms (~+1.8‰, based on the above fractionation factor from the Rayleigh model and an average surface $\delta^{30}Si_{DSi}$ of +3.2‰, 2 SD = 0.9, n = 7) are within error identical with the $\delta^{30}Si_{DSi}$ of bottom waters (~+2.0‰). As discussed in Section 4.1.1, the entire water column outside the Lena River plume is depleted in nutrients due to a combination of uptake by phytoplankton in summer and homogenization during seasonal stratification breakdown in autumn and winter. Bottom waters outside the influence of the Lena River plume have $\delta^{30}Si_{DSi}$ signatures up to ~ +1.5‰ heavier than $\delta^{30}Si_{DSi\_0}$ (Figure 5b), which is consistent with this scenario. However, the bottom samples with the highest DSi excess have the lowest $\Delta\delta^{30}Si_{DSi}$ (+0.45 and +0.16‰ for stations 7 and 6 from 2013 to 2014, respectively), which agrees with benthic Si release as the main source of [DSi] excess. Elevated benthic Si fluxes have been inferred for the Siberian Interior Shelf Seas and other shallow regions of the Arctic Ocean (Brzezinski et al., 2021; März et al., 2015, 2022; Sun et al., 2021). In addition to dissolution of biogenic Si from settled diatom frustules, the dissolution of primary minerals would result in relatively light $\delta^{30}Si_{DSi}$ (Frings et al., 2016), while heavier $\delta^{30}Si_{DSi}$ signatures are expected if authigenic clay formation (Ehlert et al., 2016; Opfergelt & Delmelle, 2012) and Si adsorption onto ferric hydroxides (Zheng et al., 2016) removes lighter isotopes from pore waters. Pore water $\delta^{30}Si_{DSi}$ signatures have been determined for the Barents Sea and estimated for the Chukchi Sea at values ranging between −0.51 and +1.69‰ (Brzezinski et al., 2021; Ward et al., 2021), which is significantly lighter than the values expected for the northwestern Laptev Sea (~+1.8‰, see above), indicating that preformed $\delta^{30}Si_{DSi}$ values prior to biological production were either different or that other dissolution processes are at play in the Laptev Sea.

The excess of DIP beneath the Lena River plume in the winter samples is significantly higher than that of DSi even if the winter end-member is used (+200 to +600%). The Lena River winter end-member [DIP] (0.16 μM) of our study is based on only one sample collected in November 2011, which is marked by a lower [DIP] than river water samples taken in preceding winters (e.g., 0.52 μM in early 2011). In addition, temporally limited but exceptionally high [DIP] peaks (up to ~1.2 μM) have been observed for freshwater of the Lena River (Sanders et al., 2022). Therefore, variations in Lena River winter end-member [DIP] may partly explain the discrepancy between expected and observed [DIP] in the winter samples. The flow-weighed summer and winter Lena River inputs (2.7–8.7*10^9 g and 0.5–1.7*10^9 g, respectively; [DIP] end-member values taken from Arctic Great River Observatory or Gordeev et al., 1996) agree well with those reported by Holmes et al. (2012) and correspond to 17%–56% and 3%–11% of the DIP enrichment in the bottom layer (~15*10^9 g), respectively. Even the maximum annual DIP contribution of the Lena River (3–10*10^9 g) could account only for 68% of the DIP excess. However, redistribution through sea ice formation does not solely affect river-borne nutrients but essentially all nutrients present in the surface layer. Most of the DIP in the Laptev Sea is supplied by the advection of AAW, which makes up as much as 90% of the surface layer. Therefore, the combined redistribution of AAW-derived DIP in the water column with DIP supplied by the Lena River could be responsible for the excess in the bottom layer. DIP released during organic matter degradation may also lead to DIP excess in the bottom layer, as was recently observed for the Laptev Shelf slope (Sun et al., 2021). However, if DIP excess beneath the Lena River plume is driven by in situ benthic DIP release, a hitherto unexplored mechanism would be required to explain the much stronger accumulation of DIP during winter when temperatures and primary productivity rates are lowest. In addition, our four summer MUC samples (Section 2.1) have Δ[*nutrient*] values similar to those of the bottom water samples from the same stations, except at station 18 from 2014 at which, however, salinity also strongly differs between the MUC and the bottom water sample. These observations argue against a major role of benthic DIP contributions in generating the marked DIP excess beneath the Lena River plume. As discussed above, benthic DSi release is resolvable in our data set but confined to the outer shelf of the northwestern Laptev Sea at a depth of 50 m. Below this depth, dissolved $\delta^{30}Si_{DSi}$ can be entirely attributed to advection of AAW characterized by a $\delta^{30}Si_{DSi}$ of ~+2‰ (Varela et al., 2016), resulting in $\Delta\delta^{30}Si_{DSi}$ values around zero

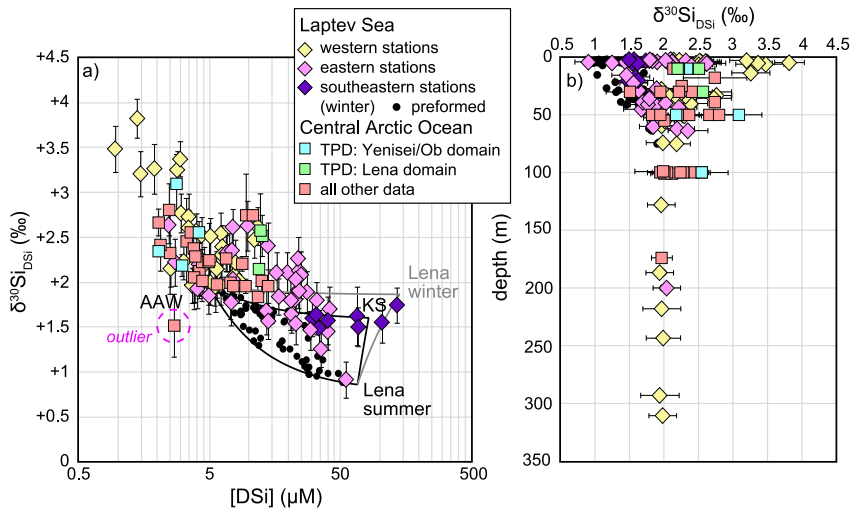

Figure 8. Si isotope signatures and [DSi] in samples from the Laptev Sea (this study, diamond symbols) compared with samples (<180 m) from the central Arctic Ocean (Liguori et al., 2021, square symbols). (a) Dissolved stable Si isotopes ($\delta^{30}Si_{DSi}$) plotted against silicic acid concentrations ([DSi]) (corresponding to Figure 5a). (b) Dissolved stable silicon isotopes ($\delta^{30}Si_{DSi}$) plotted against depth (corresponding to Figure 3). The sample of station PS94/069–5 from 30 m depth is considered an outlier in our study.

for these samples. In addition, Δ[DIP] and Δ[DSi] values of the shelf slope samples scatter around zero or are even negative (Figure 6), which supports our observation of significant benthic fluxes being restricted to a narrow area at the outer shelf of the Laptev Sea. Benthic DIP fluxes would constitute only ∼13% of the AAW contribution (Sun et al., 2021) and thus are not resolvable with our water component assessment for the highly AAW-influenced northern Laptev Sea (i.e., Δ[DIP] does not exceed zero percent outside the Lena River plume).

4.2. Implications for Nutrient Bioavailability in the Transpolar Drift

Laterally and vertically separated contributions of the Lena and Yenisei/Ob rivers have recently been identified in the central Arctic Ocean based on a semiquantitative water component analysis involving standard hydrographic parameters, radiogenic neodymium and stable oxygen isotopes as well as REEs (Paffrath et al., 2021; Figure S4 in Supporting Information S1). Both TPD freshwater domains have provenance tracer characteristics similar to those observed in the northern Laptev Sea (Laukert, Frank, Bauch, Hathorne, Gutjahr et al., 2017), in line with the Laptev Sea being the main source region of freshwater, nutrients, and trace elements transported via the TPD. The "shelf-influenced" nutrient regime with low [DIN] but high [DSi] ($[DSi]_{DIN}$* reaches ∼12 μM) in 2015 was confined to the Lena domain comprising the freshwater-rich (f_{RIV} up to ∼20%) part of the TPD (Figure S4 in Supporting Information S1). The persistent stratification in the southeastern Laptev Sea limits vertical nitrogen flux and thus inhibits the complete consumption of DSi supplied by the Lena River, which instead is exported via the Lena domain through the northeastern Laptev Sea. The origin of the "shelf-influenced" nutrient regime from the eastern Laptev Sea is further supported by the close correspondence of [DSi] and $\delta^{30}Si_{DSi}$ characteristics between the Lena domain of the TPD (Liguori et al., 2021) and the waters prevailing in the eastern Laptev Sea (Figure 8a). The relatively homogenous DSi distributions observed within and below this shallower TPD domain likely result from combined DSi utilization at the surface and DSi enrichment in the bottom layer through sea ice formation in winter. Both processes overprint the DSi distributions expected from water mass mixing (i.e., high [DSi] at surface due to Lena River inputs and low [DSi] in bottom layer due to AAW dominance). This is supported by lighter signatures in TPD waters below the Lena domain reaching +1.83‰ at 50 m depth in agreement with relatively light $\delta^{30}Si_{DSi}$ winter inputs from the Lena River and heavier signatures of ∼+2.5‰ in surface waters of the Lena domain resulting from DSi utilization (Figure S4 in Supporting Information S1). In years with direct northward Lena River plume advection (e.g., in 2013), the majority of river-borne DSi is exported offshore, while weaker export occurs in years with eastward deflection of the Lena River plume (e.g., in 2014). The difference between north- and eastward deflection of the Lena River plume is consistent with the spatiotemporal variability in provenance tracer distributions observed within the TPD (Paffrath et al., 2021).

In contrast to the Lena domain of the TPD, the domain containing contributions from the Yenisei and Ob rivers (f_{RIV} reaches up to 6%) has low [DSi] and [DIN] ($[DSi]_{DIN}$* near zero μM) (Figure S4 in Supporting Information S1). These nutrient characteristics define the "Polar" nutrient regime (Fernández-Méndez et al., 2015; Flores et al., 2019), which can only be established via strong utilization of river-borne DSi enabled by replenishment of AAW-derived DIN (Section 4.1.1). Such a strong utilization is enabled by the long transit times of Yenisei/Ob-derived nutrients from the southern Kara Sea to the central Arctic Ocean and by the strong upward supply of DIN during erosion of the stratification in late autumn and early winter (see also Janout et al., 2016). Seasonal erosion of the stratification only occurs outside the river plumes and therefore is largely confined to the northern Kara Sea and the northwestern Laptev Sea, the main source areas of the Yenisei/Ob domain (Paffrath et al., 2021). Similar to the "shelf-influenced" nutrient regime, the origin of the "Polar" nutrient regime from the western Laptev Sea is confirmed by similar [DSi] and $\delta^{30}Si$ characteristics of the Yenisei/Ob domain of the TPD (Liguori et al., 2021) and the waters prevailing in the western Laptev Sea (Figure 8a). The "Polar" nutrient regime also prevailed at the margin of the Barents Sea in 2015 (Figure S4 in Supporting Information S1) in waters with significantly lower REEs (Paffrath et al., 2021), which agrees with direct advection of these waters from the Barents Sea (Laukert et al., 2019).

Overall, the distribution of [DSi] and $\delta^{30}Si_{DSi}$ composition within the TPD (see Brzezinski et al., 2021; Liguori et al., 2021) can be attributed to nutrient export from the Laptev Sea, which in turn suggests that biological or biogeochemical processes along the TPD do not significantly alter the [DSi] distribution. The $\delta^{30}Si_{DSi}$ signatures within the Yenisei/Ob domain of the TPD reach +3.09‰ at 50 m depth (Liguori et al., 2021) and thus in waters with highest Yenisei/Ob contributions (Paffrath et al., 2021, Figure S4 in Supporting Information S1), which agrees with strong DSi drawdown in the western Laptev Sea prior to export of these shelf waters via the TPD. In contrast, as mentioned above, the Lena domain is marked by lighter signatures at 50 m depth and heavier signatures of ∼+2.5‰ in surface waters (Liguori et al., 2021). Liguori et al. (2021) attributed the heavier $\delta^{30}Si_{DSi}$ values at the surface to DSi utilization by sea ice diatoms or sea ice-attached diatoms along the TPD. However, the matching $\delta^{30}Si_{DSi}$ signatures of the Lena domain samples from the TPD and the samples of the eastern Laptev Sea collected in the frame of our study suggest that the uptake of DSi may have occurred already in the ice-free Laptev Sea prior to nutrient export via the TPD. The only difference between the two $\delta^{30}Si_{DSi}$ data sets are the heavier $\delta^{30}Si_{DSi}$ signatures encountered at 50 and 100 m depth in the Yenisei/Ob domain and in waters outside the TPD influence (Figure 8b). Heavier $\delta^{30}Si_{DSi}$ signatures in the Yenisei/Ob domain could be explained by enhanced vertical mixing at the outer Laptev Shelf, which is only partly covered by our data. Such mixing enables transport of the heavy surface $\delta^{30}Si_{DSi}$ signatures observed in the northwestern Laptev Sea to deeper layers, which in turn causes lower $\delta^{30}Si_{DSi}$ signatures in the surface layer of the Yenisei/Ob domain (+2.34‰) than in the surface layer of the northwestern Laptev Sea (∼+3.5‰). The heavy signatures outside the TPD influence are confined to the "Atlantic" nutrient regime. However, provenance tracer data suggest that these waters were partly also modified by admixture of shelf waters from the Kara Sea (Paffrath et al., 2021 and Figure S4 in Supporting Information S1) but to a much lesser extent than the waters advected via the Yenisei/Ob domain. Therefore, the admixture of productive nutrient depleted waters from the Kara Sea could account for the heavier $\delta^{30}Si_{DSi}$ signatures in the central Arctic Ocean at 50–100 m depths. One sample from the central Arctic Ocean (PS94/069–5, 30 m depth, Liguori et al., 2021) clearly differs from all other samples of the data set and also does not reflect the [DSi]-$\delta^{30}Si_{DSi}$ properties of the Laptev Sea shelf waters, which is why we excluded it from our discussion (Figure 8).

In 2012, the "Polar" nutrient regime covered a larger area in the central Arctic Ocean than in 2015 (Fernández-Méndez et al., 2015; Flores et al., 2019). This indicates that prior to the sampling campaign in 2012, the Lena River plume was either deflected to the east as was observed in 2014 or that a greater reduction of stratification in the eastern Laptev Sea allowed for enhanced biological uptake of DSi supplied by the Lena River. Both scenarios are consistent with the strong interannual variability of the Laptev Sea hydrography (Janout et al., 2020), mainly driven by changing wind fields causing differences in Lena River plume extent or strength of stratification. Therefore, it is the variability in the Laptev Sea hydrography and nutrient biogeochemistry that defines the distribution of the different nutrient regimes within the TPD. This is an important observation considering that the central Arctic Ocean will likely be ice-free in summer before the middle of this century (Notz & Community, 2020), resulting in higher exposure of the surface layer to solar irradiance and wind stress and potentially stronger stimulation of photosynthesis via enhanced light and nutrient bioavailability. However, if stratification in the Laptev Sea continues to weaken (Janout et al., 2020), river-bound DSi and other nutrients are more

likely to be consumed on the shelves and thus prior to their export. This would result in strong lateral gradients of the future biological regimes between the central Arctic Ocean, the inner Laptev Sea shelf, and the continental slope region, which receives AW-sourced nutrients with the boundary current and is projected to experience a future increase in productivity due to progressing Atlantification (i.e., the increasing influence of Atlantic waters) along with further reduction in stratification (Bluhm et al., 2020; Oziel et al., 2022; Schulz et al., 2022). The loss of sea ice will therefore only lead to stronger diatom-dominated primary productivity in the central Arctic Ocean for a short period of time, if at all. DSi limitation has previously been observed in the eastern Fram Strait and the Nansen Basin and has been attributed to the presence of Atlantic water (Fernández-Méndez et al., 2015; Krisch et al., 2020). A negative trend in surface [DSi] has also been observed in recent decades in the subpolar North Atlantic Ocean (Hátún et al., 2017), the Barents Sea (Rey, 2012), and the (A)AW-influenced sector of the Nansen Basin (Duarte et al., 2021), suggesting that ongoing changes within the "Atlantic" nutrient regime favor DSi limitation. On the other hand, our data underscore the importance of the progressive weakening of stratification and an associated increase in diatom productivity and DSi utilization in the Laptev Sea for the increasing expansion of the "polar" nutrient regime at the expense of the "shelf-influenced" regime. We suggest that this process will not only counteract but also outweigh the predicted increase in riverine DSi supply and a potential intensification of Si remineralization. Remineralization of Si from settling diatoms currently is limited in the Laptev Sea, as indicated by our data and a preliminary Si isotope budget for the Arctic Ocean, suggesting removal of DSi with light $\delta^{30}Si_{DSi}$ on the shelves (Brzezinski et al., 2021). We also do not anticipate a strong intensification in remineralization, given that the high sedimentation rates, particularly in the southern Laptev Sea, should generally favor lower biogenic Si exposure to dissolution and burial. Therefore, the changes anticipated for the Laptev Sea are expected to add to the increasing limitation of bioavailable DSi observed in different regions of the Arctic Ocean.

5. Conclusions

We provide new insights into the nutrient dynamics of the Laptev Sea and assess its importance for nutrient bioavailability along the TPD. Evaluation of water column nutrient and Si isotope distributions of the late summers of 2013 and 2014 and the winter of 2012 in combination with a water component analysis based on provenance tracers suggests that the Laptev Sea is a highly efficient trap particularly for DSi despite the high DSi flux from the Lena River and benthic DSi inputs. The efficient removal of DSi is enabled by DIN replenishment from the deep marine pool, which stimulates diatom-dominated primary productivity in the Laptev Sea well beyond river-borne DIN removal and causes pronounced drawdowns of all macronutrients at the surface as well as beneath the pycnocline in areas outside the Lena River plume. Our Si isotope data and the above observations support efficient removal of light $\delta^{30}Si_{DSi}$ in the Laptev Sea via fractionation during biological DSi utilization. This process has been invoked to compensate the input of light $\delta^{30}Si_{DSi}$ from river and sediment pore waters to balance the Si isotope budget of the Arctic Ocean (Brzezinski et al., 2021) and is also in line with water mass mixing being considered the dominant process controlling Si isotope distributions in the deep central Arctic Ocean (Liguori et al., 2020). The latter suggests that input and burial of isotopically light $\delta^{30}Si_{DSi}$ signatures a confined to the Siberian Interior Shelf Seas. Biological Si utilization in the Laptev Sea is therefore an important process whose influence on the $\delta^{30}Si_{DSi}$ as well as the [DIN], [DIP], and [DSi] distributions extends far beyond the Siberian Shelf.

The establishment of the "shelf-influenced" and "Polar" nutrient regimes exported via the TPD is controlled by combined conservative and nonconservative processes occurring in different regions of the Laptev Sea. In particular, the interplay between stratification, marine (mainly DIN and DIP) and riverine (mainly DSi) nutrient inputs and diatom-dominated primary productivity results in strong seasonally and interannually variable nutrient gradients. The retreat of the "shelf-influenced" nutrient regime, which we invoke based on our newly gained understanding of the Laptev Sea biogeochemistry combined with recent observations of a progressively weakening stratification (Janout et al., 2020), will eventually reduce diatom-dominated primary productivity in the TPD. This reduction will result in a shift toward haptophyte-dominated phytoplankton compositions in the central Arctic Ocean and significant alterations of organic carbon export to the bathypelagic layer (Tréguer et al., 2017). The anticipated increase in DSi supply via the Siberian rivers will counteract this process but we expect that the increase in DSi utilization and subsequent Si burial will outweigh riverine supply, which will result in lower rather than higher DSi export to the central Arctic Ocean and the North Atlantic. The exact interplay between Laptev Sea hydrography and nutrient biogeochemistry remains to be fully explored in dedicated process studies

to enable reliable forecasts of nutrient bioavailability in the Laptev Sea, the central Arctic Ocean, and the North Atlantic.

Conflict of Interest

The authors declare no conflicts of interest relevant to this study.

Data Availability Statement

Maps and figures were produced using Ocean Data View and Microsoft Excel, respectively. All data presented in this study have been included in the Supporting Information (Data sets S1 and S2 in Supporting Information S1) and, in addition, have been published in the PANGAEA database (for 2012: Novikhin, Dobrotina, Kirillov et al., 2021, https://doi.pangaea.de/10.1594/PANGAEA.931257; for 2013: Novikhin, Povazhnyi, Dobrotina, Ipatov et al., 2021, https://doi.pangaea.de/10.1594/PANGAEA.931240; for 2014: Novikhin, Povazhnyi, Dobrotina, Morozova et al., 2021, https://doi.pangaea.de/10.1594/PANGAEA.931209; Si isotope and complementary data for all years: Laukert et al., 2021, https://doi.pangaea.de/10.1594/PANGAEA.938259).

Acknowledgments
We like to thank the Captain and Crew of the RV Viktor Buynitskiy and all members of the project "Laptev Sea System" for their help in collecting and transporting the samples. We also acknowledge Jutta Heinze and Andre Mutzberg (GEOMAR) for laboratory assistance and DSi analysis in the isotope samples, respectively. Financial support for the "Laptev Sea System" project was provided by the German Federal Ministry of Education and Research (Grant BMBF 03F0776 and 03G0833) and the Ministry of Education and Science of the Russian Federation. G. L. also acknowledges financial support through the Ocean Frontier Institute through an award from the Canada First Research Excellence Fund. Open Access funding enabled and organized by Projekt DEAL.

References

Ardyna, M., & Arrigo, K. R. (2020). Phytoplankton dynamics in a changing Arctic Ocean. *Nature Climate Change*, *10*(10), 892–903. https://doi.org/10.1038/s41558-020-0905-y

Arrigo, K. R., & van Dijken, G. L. (2015). Continued increases in Arctic Ocean primary production. *Progress in Oceanography*, *136*, 60–70. https://doi.org/10.1016/j.pocean.2015.05.002

Bauch, D., & Cherniavskaia, E. (2018). Water mass classification on a highly variable Arctic shelf region: Origin of Laptev Sea water masses and implications for the nutrient budget. *Journal of Geophysical Research: Oceans*, *123*(3), 1896–1906. https://doi.org/10.1002/2017jc013524

Bauch, D., Dmitrenko, I. A., Wegner, C., Holemann, J., Kirillov, S. A., Timokhov, L. A., & Kassens, H. (2009). Exchange of Laptev Sea and Arctic Ocean halocline waters in response to atmospheric forcing. *Journal of Geophysical Research*, *114*(C5), C05008. https://doi.org/10.1029/2008jc005062

Bauch, D., Holemann, J., Willmes, S., Groger, M., Novikhin, A., Nikulina, A., et al. (2010). Changes in distribution of brine waters on the Laptev Sea shelf in 2007. *Journal of Geophysical Research*, *115*(C11), C11008. https://doi.org/10.1029/2010jc006249

Bauch, D., Hölemann, J. A., Dmitrenko, I. A., Janout, M. A., Nikulina, A., Kirillov, S. A., et al. (2012). Impact of Siberian coastal polynyas on shelf-derived Arctic Ocean halocline waters. *Journal of Geophysical Research*, *117*(C9), C00G12. https://doi.org/10.1029/2011jc007282

Bauch, D., Hölemann, J., Andersen, N., Dobrotina, E., Nikulina, A., & Kassens, H. (2011). The Arctic shelf regions as a source of freshwater and brine-enriched waters as revealed from stable oxygen isotopes. *Polarforschung*, *80*(3), 127–140.

Bauch, D., Torres-Valdes, S., Polyakov, I., Novikhin, A., Dmitrenko, I., McKay, J., & Mix, A. (2014). Halocline water modification and along-slope advection at the Laptev Sea continental margin. *Ocean Science*, *10*(1), 141–154. https://doi.org/10.5194/os-10-141-2014

Becker, S., Aoyama, M., Woodward, E. M. S., Bakker, K., Coverly, S., Mahaffey, C., & Tanhua, T. (2020). GO-SHIP repeat hydrography nutrient manual: The precise and accurate determination of dissolved inorganic nutrients in seawater, using continuous flow analysis methods. *Frontiers in Marine Science*, *7*, 908. https://doi.org/10.3389/fmars.2020.581790

Bluhm, B. A., Janout, M. A., Danielson, S., Ellingsen, I., Gavrilo, M., Grebmeier, J. M., et al. (2020). The pan-Arctic continental slope: Sharp gradients of physical processes affect pelagic and benthic ecosystems. *Frontiers in Marine Science*, *7*. https://doi.org/10.3389/fmars.2020.544386

Blunden, J., & Arndt, D. S. (2019). State of the climate in 2018. *Bulletin of the American Meteorological Society*, *100*(9). https://doi.org/10.1175/2019BAMSStateoftheClimate.1

Brzezinski, M. A. (1985). The Si:C:N ratio of marine diatoms: Interspecific variability and the effect of some environmental variables. *Journal of Phycology*, *21*(3), 347–357. https://doi.org/10.1111/j.0022-3646.1985.00347.x

Brzezinski, M. A., Closset, I., Jones, J. L., de Souza, G. F., & Maden, C. (2021). New constraints on the physical and biological controls on the silicon isotopic composition of the Arctic Ocean. *Frontiers in Marine Science*, *8*. https://doi.org/10.3389/fmars.2021.699762

Cauwet, G., & Sidorov, I. (1996). The biogeochemistry of Lena River: Organic carbon and nutrients distribution. *Marine Chemistry*, *53*(3–4), 211–227. https://doi.org/10.1016/0304-4203(95)00090-9

Charette, M. A., Kipp, L. E., Jensen, L. T., Dabrowski, J. S., Whitmore, L. M., Fitzsimmons, J. N., et al. (2020). The transpolar drift as a source of riverine and shelf-derived trace elements to the central Arctic Ocean. *Journal of Geophysical Research: Oceans*, *125*(5). https://doi.org/10.1029/2019jc015920

Codispoti, L. A., & Richards, F. A. (1968). Micronutrient distributions in the East Siberian and Laptev seas during summer 1963. *Arctic*, *21*(2). https://doi.org/10.14430/arctic3251

Codispoti, L. A., Kelly, V., Thessen, A., Matrai, P., Suttles, S., Hill, V., et al. (2013). Synthesis of primary production in the Arctic Ocean: III. Nitrate and phosphate based estimates of net community production. *Progress in Oceanography*, *110*, 126–150. https://doi.org/10.1016/j.pocean.2012.11.006

Cremer, H. (1999). Distribution patterns of diatom surface sediment assemblages in the Laptev Sea (Arctic Ocean). *Marine Micropaleontology*, *38*(1), 39–67. https://doi.org/10.1016/s0377-8398(99)00037-7

de la Rocha, C. L., Brzezinski, M. A., & DeNiro, M. J. (1997). Fractionation of silicon isotopes by marine diatoms during biogenic silica formation. *Geochimica et Cosmochimica Acta*, *61*(23), 5051–5056. https://doi.org/10.1016/s0016-7037(97)00300-1

de Souza, G. F., Reynolds, B. C., Rickli, J., Frank, M., Saito, M. A., Gerringa, L. J. A., & Bourdon, B. (2012). Southern ocean control of silicon stable isotope distribution in the deep Atlantic Ocean. *Global Biogeochemical Cycles*, *26*(2), GB2035. https://doi.org/10.1029/2011gb004141

Debyser, M. C. F., Pichevin, L., Tuerena, R. E., Dodd, P. A., Doncila, A., & Ganeshram, R. S. (2022). Tracing the role of Arctic shelf processes in Si and N cycling and export through the Fram Strait: Insights from combined silicon and nitrate isotopes. EGUsphere [preprint]. https://doi.org/10.5194/egusphere-2022-254

Demidov, A. B., Mosharov, S. A., & Makkaveev, P. N. (2014). Patterns of the Kara Sea primary production in autumn: Biotic and abiotic forcing of subsurface layer. *Journal of Marine Systems*, *132*, 130–149. https://doi.org/10.1016/j.jmarsys.2014.01.014

Demidov, A. B., Sheberstov, S. V., & Gagarin, V. I. (2020). Interannual variability of primary production in the Laptev Sea. *Oceanology*, *60*(1), 50–61. https://doi.org/10.1134/s0001437020010075

Demidov, A. B., Sheberstov, S. V., & Gagarin, V. I. (2021). Seasonal variability and annual primary production of phytoplankton in the Laptev Sea assessed by MODIS-aqua data. *Izvestiya - Atmospheric and Oceanic Physics*, *56*(9), 950–962. https://doi.org/10.1134/s000143382009008x

Dittmar, T., & Kattner, G. (2003). The biogeochemistry of the river and shelf ecosystem of the Arctic Ocean: A review. *Marine Chemistry*, *83*(3–4), 103–120. https://doi.org/10.1016/s0304-4203(03)00105-1

Duarte, P., Meyer, A., & Moreau, S. (2021). Nutrients in water masses in the Atlantic sector of the Arctic Ocean: Temporal trends, mixing and links with primary production. *Journal of Geophysical Research: Oceans*, *126*(8). https://doi.org/10.1029/2021jc017413

Ehlert, C., Doering, K., Wallmann, K., Scholz, F., Sommer, S., Grasse, P., et al. (2016). Stable silicon isotope signatures of marine pore waters - biogenic opal dissolution versus authigenic clay mineral formation. *Geochimica et Cosmochimica Acta*, *191*, 102–117. https://doi.org/10.1016/j.gca.2016.07.022

Ehlert, C., Grasse, P., Mollier-Vogel, E., Böschen, T., Franz, J., de Souza, G. F., et al. (2012). Factors controlling the silicon isotope distribution in waters and surface sediments of the Peruvian coastal upwelling. *Geochimica et Cosmochimica Acta*, *99*, 128–145. https://doi.org/10.1016/j.gca.2012.09.038

Fahl, K., Cremer, H., Erlenkeuser, H., Hanssen, H., Hölemann, J., Kassens, H., et al. (2001). Sources and pathways of organic carbon in the modern Laptev Sea (Arctic Ocean): Implication from biological, geochemical and geological data. *Polarforschung*, *69*, 193–205.

Fernández-Méndez, M., Katlein, C., Rabe, B., Nicolaus, M., Peeken, I., Bakker, K., et al. (2015). Photosynthetic production in the central Arctic Ocean during the record sea-ice minimum in 2012. *Biogeosciences*, *12*(11), 3525–3549. https://doi.org/10.5194/bg-12-3525-2015

Flores, H., David, C., Ehrlich, J., Hardge, K., Kohlbach, D., Lange, B. A., et al. (2019). Sea-ice properties and nutrient concentration as drivers of the taxonomic and trophic structure of high-Arctic protist and metazoan communities. *Polar Biology*, *42*(7), 1377–1395. https://doi.org/10.1007/s00300-019-02526-z

Frings, P. J., Clymans, W., Fontorbe, G., De La Rocha, C. L., & Conley, D. J. (2016). The continental Si cycle and its impact on the ocean Si isotope budget. *Chemical Geology*, *425*, 12–36. https://doi.org/10.1016/j.chemgeo.2016.01.020

Fritz, M., Vonk, J. E., & Lantuit, H. (2017). Collapsing Arctic coastlines. *Nature Climate Change*, *7*(1), 6–7. https://doi.org/10.1038/nclimate3188

Georg, R. B., Reynolds, B. C., Frank, M., & Halliday, A. N. (2006). New sample preparation techniques for the determination of Si isotopic compositions using MC-ICPMS. *Chemical Geology*, *235*(1–2), 95–104. https://doi.org/10.1016/j.chemgeo.2006.06.006

Giesbrecht, K. E., & Varela, D. E. (2021). Summertime biogenic silica production and silicon limitation in the Pacific Arctic region from 2006 to 2016. *Global Biogeochemical Cycles*, *35*(1). https://doi.org/10.1029/2020gb006629

Giesbrecht, K. E., Varela, D. E., de Souza, G. F., & Maden, C. (2022). Natural variations in dissolved silicon isotopes across the Arctic Ocean from the Pacific to the Atlantic. *Global Biogeochemical Cycles*, *36*(5), e2021GB007107. https://doi.org/10.1029/2021GB007107

Gordeev, V. V., & Sidorov, I. S. (1993). Concentrations of major elements and their outflow into the Laptev Sea by the Lena River. *Marine Chemistry*, *43*(1–4), 33–45. https://doi.org/10.1016/0304-4203(93)90214-9

Gordeev, V. V., Martin, J. M., Sidorov, I. S., & Sidorova, M. V. (1996). A reassessment of the Eurasian river input of water, sediment, major elements, and nutrients to the Arctic Ocean. *American Journal of Science*, *296*(6), 664–691. https://doi.org/10.2475/ajs.296.6.664

Grasse, P., Brzezinski, M. A., Cardinal, D., de Souza, G. F., Andersson, P., Closset, I., et al. (2017). GEOTRACES inter-calibration of the stable silicon isotope composition of dissolved silicic acid in seawater. *Journal of Analytical Atomic Spectrometry*, *32*(3), 562–578. https://doi.org/10.1039/c6ja00302h

Grasse, P., Ehlert, C., & Frank, M. (2013). The influence of water mass mixing on the dissolved Si isotope composition in the Eastern Equatorial Pacific. *Earth and Planetary Science Letters*, *380*, 60–71. https://doi.org/10.1016/j.epsl.2013.07.033

Grasshoff, K., Kremling, K., & Ehrhardt, M. (1999). *Methods of seawater analysis*. John Wiley & Sons.

Heim, B., Abramova, E., Doerffer, R., Günther, F., Hölemann, J., Kraberg, A., et al. (2014). Ocean colour remote sensing in the southern Laptev Sea: Evaluation and applications. *Biogeosciences*, *11*(15), 4191–4210. https://doi.org/10.5194/bg-11-4191-2014

Heiskanen, A. S., & Keck, A. (1996). Distribution and sinking rates of phytoplankton, detritus, and particulate biogenic silica in the Laptev Sea and Lena River (Arctic Siberia). *Marine Chemistry*, *53*(3–4), 229–245. https://doi.org/10.1016/0304-4203(95)00091-7

Hill, V. J., Matrai, P. A., Olson, E., Suttles, S., Steele, M., Codispoti, L. A., & Zimmerman, R. C. (2013). Synthesis of integrated primary production in the Arctic Ocean: II. In situ and remotely sensed estimates. *Progress in Oceanography*, *110*, 107–125. https://doi.org/10.1016/j.pocean.2012.11.005

Holmes, R. M., McClelland, J. W., Peterson, B. J., Tank, S. E., Bulygina, E., Eglinton, T. I., et al. (2012). Seasonal and annual fluxes of nutrients and organic matter from large rivers to the Arctic Ocean and surrounding seas. *Estuaries and Coasts*, *35*(2), 369–382. https://doi.org/10.1007/s12237-011-9386-6

Hughes, H. J., Delvigne, C., Korntheuer, M., de Jong, J., André, L., & Cardinal, D. (2011). Controlling the mass bias introduced by anionic and organic matrices in silicon isotopic measurements by MC-ICP-MS. *Journal of Analytical Atomic Spectrometry*, *26*(9), 1892–1896. https://doi.org/10.1039/C1JA10110B

Hátún, H., Azetsu-Scott, K., Somavilla, R., Rey, F., Johnson, C., Mathis, M., et al. (2017). The subpolar gyre regulates silicate concentrations in the North Atlantic. *Scientific Reports*, *7*(1), 14576. https://doi.org/10.1038/s41598-017-14837-4

Hölemann, J. A., Juhls, B., Bauch, D., Janout, M., Koch, B. P., & Heim, B. (2021). The impact of the freeze–melt cycle of land-fast ice on the distribution of dissolved organic matter in the Laptev and East Siberian seas (Siberian Arctic). *Biogeosciences*, *18*(12), 3637–3655. https://doi.org/10.5194/bg-18-3637-2021

Hölemann, J. A., Kirillov, S., Klagge, T., Novikhin, A., Kassens, H., & Timokhov, L. (2011). Near-bottom water warming in the Laptev Sea in response to atmospheric and sea-ice conditions in 2007. *Polar Research*, *30*(1), 6425. https://doi.org/10.3402/polar.v30i0.6425

IPCC. (2022). In H.-O., Pörtner, D. C., Roberts, M., Tignor, E. S., Poloczanska, K., Mintenbeck, A., Alegría, et al. (Eds.), *Climate change 2022: Impacts, adaptation, and vulnerability. Contribution of working group II to the sixth assessment report of the intergovernmental panel on climate change*. Cambridge University Press. in press.

Janout, M. A., Aksenov, Y., Hölemann, J. A., Rabe, B., Schauer, U., Polyakov, I. V., et al. (2015). Kara sea freshwater transport through vilkitsky strait: Variability, forcing, and further pathways toward the Western Arctic Ocean from a model and observations. *Journal of Geophysical Research: Oceans*, *120*(7), 4925–4944. https://doi.org/10.1002/2014jc010635

Janout, M. A., Holemann, J., & Krumpen, T. (2013). Cross-shelf transport of warm and saline water in response to sea ice drift on the Laptev Sea shelf. *Journal of Geophysical Research: Oceans*, *118*(2), 563–576. https://doi.org/10.1029/2011jc007731

Janout, M. A., Hölemann, J., Laukert, G., Smirnov, A., Krumpen, T., Bauch, D., & Timokhov, L. (2020). On the variability of stratification in the freshwater-influenced Laptev Sea region. *Frontiers in Marine Science*, *7*. https://doi.org/10.3389/fmars.2020.543489

Janout, M. A., Hölemann, J., Timokhov, L., Gutjahr, O., & Heinemann, G. (2017). Circulation in the northwest Laptev Sea in the eastern Arctic Ocean: Crossroads between Siberian River water, Atlantic water and polynya-formed dense water. *Journal of Geophysical Research: Oceans*, *122*(8), 6630–6647. https://doi.org/10.1002/2017jc013159

Janout, M., Holemann, J., Juhls, B., Krumpen, T., Rabe, B., Bauch, D., et al. (2016). Episodic warming of near-bottom waters under the Arctic sea ice on the central Laptev Sea shelf. *Geophysical Research Letters*, *43*(1), 264–272. https://doi.org/10.1002/2015gl066565

Karl, D. M., & Tien, G. (1992). MAGIC: A sensitive and precise method for measuring dissolved phosphorus in aquatic environments. *Limnology & Oceanography*, *37*(1), 105–116. https://doi.org/10.4319/lo.1992.37.1.0105

Kassens, H., & Volkmann-Lark, K. (2013). *Russian-German cooperation Laptev Sea system: TRANSDRIFT XXI expedition, August 22-September 21, 2013, cruise Report* (p. 178). Kiel, Getrennte Zählg.

Kattner, G., Lobbes, J. M., Fitznar, H. P., Engbrodt, R., Nöthig, E. M., & Lara, R. J. (1999). Tracing dissolved organic substances and nutrients from the Lena River through Laptev Sea (Arctic). *Marine Chemistry*, *65*(1–2), 25–39. https://doi.org/10.1016/s0304-4203(99)00008-0

Klunder, M. B., Bauch, D., Laan, P., de Baar, H. J. W., van Heuven, S., & Ober, S. (2012). Dissolved iron in the Arctic shelf seas and surface waters of the central Arctic Ocean: Impact of Arctic river water and ice-melt. *Journal of Geophysical Research*, *117*(C1). https://doi.org/10.1029/2011jc007133

Krause, J. W., Schulz, I. K., Rowe, K. A., Dobbins, W., Winding, M. H. S., Sejr, M. K., et al. (2019). Silicic acid limitation drives bloom termination and potential carbon sequestration in an Arctic bloom. *Scientific Reports*, *9*(1), 8149. https://doi.org/10.1038/s41598-019-44587-4

Krisch, S., Browning, T. J., Graeve, M., Ludwichowski, K. U., Lodeiro, P., Hopwood, M. J., et al. (2020). The influence of Arctic Fe and Atlantic fixed N on summertime primary production in Fram Strait, North Greenland Sea. *Scientific Reports*, *10*(1), 15230. https://doi.org/10.1038/s41598-020-72100-9

Laukert, G., Frank, M., Bauch, D., Hathorne, E. C., Gutjahr, M., Janout, M., & Hölemann, J. (2017). Transport and transformation of riverine neodymium isotope and rare Earth element signatures in high latitude estuaries: A case study from the Laptev Sea. *Earth and Planetary Science Letters*, *477*, 205–217. https://doi.org/10.1016/j.epsl.2017.08.010

Laukert, G., Frank, M., Bauch, D., Hathorne, E. C., Rabe, B., von Appen, W. J., et al. (2017). Ocean circulation and freshwater pathways in the Arctic Mediterranean based on a combined Nd isotope, REE and oxygen isotope section across Fram Strait. *Geochimica et Cosmochimica Acta*, *202*, 285–309. https://doi.org/10.1016/j.gca.2016.12.028

Laukert, G., Frank, M., Hathorne, E. C., Krumpen, T., Rabe, B., Bauch, D., et al. (2017). Pathways of Siberian freshwater and sea ice in the Arctic Ocean traced with radiogenic neodymium isotopes and rare Earth elements. *Polarforschung*, *87*, 3–13. https://doi.org/10.2312/polarforschung.87.1.3

Laukert, G., Grasse, P., Doering, K., Frank, M., Kassens, H., & Timokhov, L. (2021). *Dissolved stable silicon isotopes measured on water bottle samples collected during TRANSDRIFT-XX (TI12, 2012), TRANSDRIFT-XXI (VB13, 2013) and TRANSDRIFT-XXII (VB14, 2014)*, Laptev Sea. *PANGAEA*, https://doi.org/10.1594/PANGAEA.938259

Laukert, G., Makhotin, M., Petrova, M. V., Frank, M., Hathorne, E. C., Bauch, D., et al. (2019). Water mass transformation in the Barents Sea inferred from radiogenic neodymium isotopes, rare Earth elements and stable oxygen isotopes. *Chemical Geology*, *511*, 416–430. https://doi.org/10.1016/j.chemgeo.2018.10.002

Le Fouest, V., Babin, M., & Tremblay, J. É. (2013). The fate of riverine nutrients on Arctic shelves. *Biogeosciences*, *10*(6), 3661–3677. https://doi.org/10.5194/bg-10-3661-2013

Lewis, K. M., van Dijken, G. L., & Arrigo, K. R. (2020). Changes in phytoplankton concentration now drive increased Arctic Ocean primary production. *Science*, *369*(6500), 198–202. https://doi.org/10.1126/science.aay8380

Liguori, B. T. P., Ehlert, C., & Pahnke, K. (2020). The influence of water mass mixing and particle dissolution on the silicon cycle in the central Arctic Ocean. *Frontiers in Marine Science*, *7*. https://doi.org/10.3389/fmars.2020.00202

Liguori, B. T. P., Ehlert, C., Nöthig, E. M., Ooijen, J. C., & Pahnke, K. (2021). The transpolar drift influence on the Arctic Ocean silicon cycle. *Journal of Geophysical Research: Oceans*, *126*(11). https://doi.org/10.1029/2021jc017352

Létolle, R., Martin, J. M., Thomas, A. J., Gordeev, V. V., Gusarova, S., & Sidorov, I. S. (1993). 18O abundance and dissolved silicate in the Lena delta and Laptev Sea (Russia). *Marine Chemistry*, *43*(1–4), 47–64. https://doi.org/10.1016/0304-4203(93)90215-a

MacDonald, R. W., Anderson, L. G., Christensen, J. P., Miller, L. A., Semiletov, I. P., & Stein, R. (2010). The Arctic Ocean. In K. K. Liu (Ed.), *Carbon and nutrient fluxes in continental margins* (pp. 292–303). Sperling-Verlag).

Martin, J. M., Guan, D. M., Elbaz-Poulichet, F., Thomas, A. J., & Gordeev, V. V. (1993). Preliminary assessment of the distributions of some trace elements (As, Cd, Cu, Fe, Ni, Pb and Zn) in a pristine aquatic environment: The Lena River estuary (Russia). *Marine Chemistry*, *43*(1–4), 185–199. https://doi.org/10.1016/0304-4203(93)90224-c

Mavromatis, V., Rinder, T., Prokushkin, A. S., Pokrovsky, O. S., Korets, M. A., Chmeleff, J., & Oelkers, E. H. (2016). The effect of permafrost, vegetation, and lithology on Mg and Si isotope composition of the Yenisey River and its tributaries at the end of the spring flood. *Geochimica et Cosmochimica Acta*, *191*, 32–46. https://doi.org/10.1016/j.gca.2016.07.003

Meiners, K. M., & Michel, C. (2016). Dynamics of nutrients, dissolved organic matter and exopolymers in sea ice. In *Sea ice*, (Vol. 3), In D. N. Thomas (Ed.), (pp.415–432). https://doi.org/10.1002/9781118778371.ch17

Meyerink, S. W., Ellwood, M. J., Maher, W. A., Dean Price, G., & Strzepek, R. F. (2017). Effects of iron limitation on silicon uptake kinetics and elemental stoichiometry in two Southern Ocean diatoms, Eucampia Antarctica and Proboscia inermis, and the temperate diatom Thalassiosira pseudonana. *Limnology & Oceanography*, *62*(6), 2445–2462. https://doi.org/10.1002/lno.10578

Middag, R., de Baar, H. J. W., Laan, P., & Klunder, M. B. (2011). Fluvial and hydrothermal input of manganese into the Arctic Ocean. *Geochimica et Cosmochimica Acta*, *75*(9), 2393–2408. https://doi.org/10.1016/j.gca.2011.02.011

Milligan, A. J., Varela, D. E., Brzezinski, M. A., & Morel, F. M. M. (2004). Dynamics of silicon metabolism and silicon isotopic discrimination in a marine diatomas a function of pCO_2. *Limnology & Oceanography*, *49*(2), 322–329. https://doi.org/10.4319/lo.2004.49.2.0322

Moore, C. M. (2016). Diagnosing oceanic nutrient deficiency. *Philosophical Transactions of the Royal Society A: Mathematical, Physical & Engineering Sciences*, *374*(2081), 20150290. https://doi.org/10.1098/rsta.2015.0290

Mosharov, S. A. (2010). Distribution of the primary production and chlorophyll a in the Kara Sea in September of 2007. *Oceanology*, *50*(6), 884–892. https://doi.org/10.1134/s0001437010060081

März, C., Freitas, F. S., Faust, J. C., Godbold, J. A., Henley, S. F., Tessin, A. C., et al. (2022). Biogeochemical consequences of a changing Arctic shelf seafloor ecosystem. *Ambio*, *51*(2), 370–382. https://doi.org/10.1007/s13280-021-01638-3

März, C., Meinhardt, A. K., Schnetger, B., & Brumsack, H. J. (2015). Silica diagenesis and benthic fluxes in the Arctic Ocean. *Marine Chemistry*, *171*, 1–9. https://doi.org/10.1016/j.marchem.2015.02.003

Nitishinsky, M., Anderson, L. G., & Hölemann, J. A. (2007). Inorganic carbon and nutrient fluxes on the Arctic Shelf. *Continental Shelf Research*, *27*(10–11), 1584–1599. https://doi.org/10.1016/j.csr.2007.01.019

Notz, D., & Community, S. (2020). Arctic sea ice in CMIP6. *Geophysical Research Letters*, *47*(10). https://doi.org/10.1029/2019gl086749

Novikhin, A., Dobrotina, E., Kirillov, S.A., Kassens, H., & Timokhov, L. (2021). Nutrient and oxygen concentrations measured on water bottle samples collected during helicopter/ice camp TRANSDRIFT-XX (TI12) in winter 2012, Laptev Sea. *PANGAEA*, https://doi.org/10.1594/PANGAEA.931257

Novikhin, A., Povazhnyi, V., Dobrotina, E., Ipatov, A., Kassens, H., & Timokhov, L. (2021). Nutrient and oxygen concentrations measured on water bottle samples collected during cruise TRANSDRIFT-XXI (VB13) in 2013, Laptev Sea. *PANGAEA*, https://doi.org/10.1594/PANGAEA.931240

Novikhin, A., Povazhnyi, V., Dobrotina, E., Morozova, O., Kassens, H., & Timokhov, L. (2021). Nutrient and oxygen concentrations, alkalinity and pH measured on water bottle samples collected during cruise Transdrift-XXII (VB14) in 2014, Laptev Sea. *PANGAEA*, https://doi.org/10.1594/PANGAEA.931209

Opfergelt, S., & Delmelle, P. (2012). Silicon isotopes and continental weathering processes: Assessing controls on Si transfer to the ocean. *Comptes Rendus Geoscience*, *344*(11–12), 723–738. https://doi.org/10.1016/j.crte.2012.09.006

Oziel, L., Schourup-Kristensen, V., Wekerle, C., & Hauck, J. (2022). The pan-Arctic continental slope as an intensifying conveyer belt for nutrients in the central Arctic Ocean (1985–2015). *Global Biogeochemical Cycles*, *36*(6), e2021GB007268. https://doi.org/10.1029/2021GB007268

Paffrath, R., Laukert, G., Bauch, D., Rutgers van der Loeff, M., & Pahnke, K. (2021). Separating individual contributions of major Siberian Rivers in the transpolar drift of the Arctic Ocean. *Scientific Reports*, *11*(1), 8216. https://doi.org/10.1038/s41598-021-86948-y

Pivovarov, S., Hölemann, J. A., Kassens, H., Piepenburg, D., & Schmid, M. K. (2005). Laptev and East Siberian seas. In A. R. Robinson & K. H. Brink (Eds.), *the sea* (Vol. 14, pp. 1111–1137). Harvard University Press.

Pnyushkov, A. V., Polyakov, I. V., Alekseev, G. V., Ashik, I. M., Baumann, T. M., Carmack, E. C., et al. (2021). A steady regime of volume and heat transports in the eastern Arctic Ocean in the early 21st century. *Frontiers in Marine Science*, *8*. https://doi.org/10.3389/fmars.2021.705608

Pokrovsky, O. S., Reynolds, B. C., Prokushkin, A. S., Schott, J., & Viers, J. (2013). Silicon isotope variations in Central Siberian Rivers during basalt weathering in permafrost-dominated larch forests. *Chemical Geology*, *355*, 103–116. https://doi.org/10.1016/j.chemgeo.2013.07.016

Polyakova, Y. I., Kryukova, I. M., Martynov, F. M., Novikhin, A. E., Abramova, E. N., Kassens, H., & Hölemann, J. (2021). Community structure and spatial distribution of phytoplankton in relation to hydrography in the Laptev Sea and the East Siberian Sea (autumn 2008). *Polar Biology*, *44*(7), 1229–1250. https://doi.org/10.1007/s00300-021-02873-w

Ragueneau, O., Tréguer, P., Leynaert, A., Anderson, R., Brzezinski, M., DeMaster, D., et al. (2000). A review of the Si cycle in the modern ocean: Recent progress and missing gaps in the application of biogenic opal as a paleoproductivity proxy. *Global and Planetary Change*, *26*(4), 317–365. https://doi.org/10.1016/s0921-8181(00)00052-7

Randelhoff, A., Holding, J., Janout, M., Sejr, M. K., Babin, M., Tremblay, J.-É., & Alkire, M. B. (2020). Pan-Arctic Ocean primary production constrained by turbulent nitrate fluxes. *Frontiers in Marine Science*, *7*. https://doi.org/10.3389/fmars.2020.00150

Rey, F. (2012). Declining silicate concentrations in the Norwegian and Barents seas. *ICES Journal of Marine Science*, *69*(2), 208–212. https://doi.org/10.1093/icesjms/fss007

Reyes, F. R., & Lougheed, V. L. (2018). Rapid nutrient release from permafrost thaw in Arctic aquatic ecosystems. *Arctic Antarctic and Alpine Research*, *47*(1), 35–48. https://doi.org/10.1657/aaar0013-099

Reynolds, B. C., Aggarwal, J., Andr, L., Baxter, D., Beucher, C., Brzezinski, M. A., et al. (2007). An inter-laboratory comparison of Si isotope reference materials. *Journal of Analytical Atomic Spectrometry*, *22*(5), 561–568. https://doi.org/10.1039/b616755a

Reynolds, B., Frank, M., & Halliday, A. (2006). Silicon isotope fractionation during nutrient utilization in the North Pacific. *Earth and Planetary Science Letters*, *244*(1–2), 431–443. https://doi.org/10.1016/j.epsl.2006.02.002

Rijkenberg, M. J. A., Slagter, H. A., Rutgers van der Loeff, M., van Ooijen, J., & Gerringa, L. J. A. (2018). Dissolved Fe in the deep and upper Arctic Ocean with a focus on Fe limitation in the Nansen basin. *Frontiers in Marine Science*, *5*. https://doi.org/10.3389/fmars.2018.00088

Rudels, B., Anderson, L., Eriksson, P., Fahrbach, E., Jakobsson, M., Jones, E. P., et al. (2012). Observations in the Ocean. In P. Lemke & H.-W. Jacobi (Eds.), *Arctic climate change: The ACSYS decade and beyond* (pp. 117–198). Springer Netherlands. https://doi.org/10.1007/978-94-007-2027-5_4

Sakshaug, E. (2004). Primary and secondary production in the Arctic seas. In R. Stein & R. Macdonald (Eds.), *The organic carbon cycle in the Arctic Ocean* (pp. 57–81). Springer. https://doi.org/10.1007/978-3-642-18912-8_3

Sanders, T., Fiencke, C., Fuchs, M., Haugk, C., Juhls, B., Mollenhauer, G., et al. (2022). Seasonal nitrogen fluxes of the Lena river delta. *Ambio*, *51*(2), 423–438. https://doi.org/10.1007/s13280-021-01665-0

Schulz, K., Lincoln, B., Povazhnyy, V., Rippeth, T., Lenn, Y.-D., Janout, M., et al. (2022). Increasing nutrient fluxes and mixing regime changes in the eastern Arctic Ocean. *Geophysical Research Letters*, *49*(5), e2021GL096152. https://doi.org/10.1029/2021GL096152

Slagter, H. A., Reader, H. E., Rijkenberg, M. J. A., Rutgers van der Loeff, M., de Baar, H. J. W., & Gerringa, L. J. A. (2017). Organic Fe speciation in the Eurasian basins of the Arctic Ocean and its relation to terrestrial DOM. *Marine Chemistry*, *197*, 11–25. https://doi.org/10.1016/j.marchem.2017.10.005

Soppa, M. A., Pefanis, V., Hellmann, S., Losa, S. N., Hölemann, J., Martynov, F., et al. (2019). Assessing the influence of water constituents on the radiative heating of Laptev Sea shelf waters. *Frontiers in Marine Science*, *6*. https://doi.org/10.3389/fmars.2019.00221

Sorokin, Y. I., & Sorokin, P. Y. (1996). Plankton and primary production in the Lena river estuary and in the South-Eastern Laptev Sea. *Estuarine, Coastal and Shelf Science*, *43*(4), 399–418. https://doi.org/10.1006/ecss.1996.0078

Sun, X., Humborg, C., Mörth, C. M., & Brüchert, V. (2021). The importance of benthic nutrient fluxes in supporting primary production in the Laptev and East Siberian shelf seas. *Global Biogeochemical Cycles*, *35*(7). https://doi.org/10.1029/2020gb006849

Sun, X., Mörth, C. M., Porcelli, D., Kutscher, L., Hirst, C., Murphy, M. J., et al. (2018). Stable silicon isotopic compositions of the Lena River and its tributaries: Implications for silicon delivery to the Arctic Ocean. *Geochimica et Cosmochimica Acta*, *241*, 120–133. https://doi.org/10.1016/j.gca.2018.08.044

Sun, X., Olofsson, M., Andersson, P. S., Fry, B., Legrand, C., Humborg, C., & Mörth, C.-M. (2014). Effects of growth and dissolution on the fractionation of silicon isotopes by estuarine diatoms. *Geochimica et Cosmochimica Acta*, *130*, 156–166. https://doi.org/10.1016/j.gca.2014.01.024

Sutton, J. N., Varela, D. E., Brzezinski, M. A., & Beucher, C. P. (2013). Species-dependent silicon isotope fractionation by marine diatoms. *Geochimica et Cosmochimica Acta*, *104*, 300–309. https://doi.org/10.1016/j.gca.2012.10.057

Sutton, J., André, L., Cardinal, D., Conley, D., Souza, G., Dean, J., et al. (2018). A review of the stable isotope bio-geochemistry of the global silicon cycle and its associated trace elements. *Frontiers of Earth Science*, *5*. https://doi.org/10.3389/feart.2017.00112

Tanaka, T., Guo, L., Deal, C., Tanaka, N., Whitledge, T., & Murata, A. (2004). N deficiency in a well-oxygenated cold bottom water over the Bering Sea shelf: Influence of sedimentary denitrification. *Continental Shelf Research*, *24*(12), 1271–1283. https://doi.org/10.1016/j.csr.2004.04.004

Terhaar, J., Orr, J. C., Gehlen, M., Ethé, C., & Bopp, L. (2019). Model constraints on the anthropogenic carbon budget of the Arctic Ocean. *Biogeosciences*, *16*(11), 2343–2367. https://doi.org/10.5194/bg-16-2343-2019

Terhaar, J., Torres, O., Bourgeois, T., & Kwiatkowski, L. (2021). Arctic Ocean acidification over the 21st century co-driven by anthropogenic carbon increases and freshening in the CMIP6 model ensemble. *Biogeosciences*, *18*(6), 2221–2240. https://doi.org/10.5194/bg-18-2221-2021

Thibodeau, B., Bauch, D., & Voss, M. (2017). Nitrogen dynamic in Eurasian coastal Arctic ecosystem: Insight from nitrogen isotope. *Global Biogeochemical Cycles*, *31*(5), 836–849. https://doi.org/10.1002/2016gb005593

Torres-Valdés, S., Tsubouchi, T., Bacon, S., Naveira-Garabato, A. C., Sanders, R., McLaughlin, F. A., et al. (2013). Export of nutrients from the Arctic Ocean. *Journal of Geophysical Research: Oceans*, *118*(4), 1625–1644. https://doi.org/10.1002/jgrc.20063

Tremblay, J.-É., & Gagnon, J. (2009). The effects of irradiance and nutrient supply on the productivity of Arctic waters: A perspective on climate change. In J. C. J. Nihoul & A. G. Kostianoy (Eds.), *Influence of climate change on the changing arctic and sub-Arctic conditions*. Elsevier.

Tremblay, J.-É., Anderson, L. G., Matrai, P., Coupel, P., Bélanger, S., Michel, C., & Reigstad, M. (2015). Global and regional drivers of nutrient supply, primary production and CO_2 drawdown in the changing Arctic Ocean. *Progress in Oceanography*, *139*, 171–196. https://doi.org/10.1016/j.pocean.2015.08.009

Tremblay, J.-É., Robert, D., Varela, D. E., Lovejoy, C., Darnis, G., Nelson, R. J., & Sastri, A. R. (2012). Current state and trends in Canadian arctic marine ecosystems: I. Primary production. *Climatic Change*, *115*(1), 161–178. https://doi.org/10.1007/s10584-012-0496-3

Tremblay, J.-É., Simpson, K., Martin, J., Miller, L., Gratton, Y., Barber, D., & Price, N. M. (2008). Vertical stability and the annual dynamics of nutrients and chlorophyll fluorescence in the coastal, southeast Beaufort Sea. *Journal of Geophysical Research*, *113*(C7), C07S90. https://doi.org/10.1029/2007jc004547

Tréguer, P. J., Sutton, J. N., Brzezinski, M., Charette, M. A., Devries, T., Dutkiewicz, S., et al. (2021). Reviews and syntheses: The biogeochemical cycle of silicon in the modern ocean. *Biogeosciences*, *18*(4), 1269–1289. https://doi.org/10.5194/bg-18-1269-2021

Tréguer, P., Bowler, C., Moriceau, B., Dutkiewicz, S., Gehlen, M., Aumont, O., et al. (2017). Influence of diatom diversity on the ocean biological carbon pump. *Nature Geoscience*, *11*(1), 27–37. https://doi.org/10.1038/s41561-017-0028-x

Tuschling, K. (2000). Phytoplankton ecology in the Arctic Laptev Sea - A comparison of three seasons. *Polarforschung*, *347*.

van Ooijen, J. C., Rijkenberg, M. J. A., Gerringa, L. J. A., Rabe, B., & Rutgers van der Loeff, M. M. (2016). Inorganic nutrients measured on water bottle samples during POLARSTERN cruise PS94 (ARK-XXIX/3). *PANGAEA*. https://doi.org/10.1594/PANGAEA.868396

Varela, D. E., Brzezinski, M. A., Beucher, C. P., Jones, J. L., Giesbrecht, K. E., Lansard, B., & Mucci, A. (2016). Heavy silicon isotopic composition of silicic acid and biogenic silica in Arctic waters over the Beaufort shelf and the Canada Basin. *Global Biogeochemical Cycles*, *30*(6), 804–824. https://doi.org/10.1002/2015gb005277

Ward, J., Hendry, K., Arndt, S., Faust, J., Freitas, F., Henley, S., et al. (2021). Stable silicon isotopes uncover a mineralogical control on the benthic silicon cycle in the Arctic Barents Sea. *EarthArXiv PREPRINT*. https://doi.org/10.31223/x5f04z

Wheeler, P. A., Watkins, J. M., & Hansing, R. L. (1997). Nutrients, organic carbon and organic nitrogen in the upper water column of the Arctic Ocean: Implications for the sources of dissolved organic carbon. *Deep Sea Research Part II: Topical Studies in Oceanography*, *44*(8), 1571–1592. https://doi.org/10.1016/s0967-0645(97)00051-9

Whitefield, J., Winson, P., McClelland, J., & Menemenlis, D. (2015). A new river discharge and river temperature climatology data set for the pan-Arctic region. *Ocean Modelling*, *88*, 1–15. https://doi.org/10.1016/j.ocemod.2014.12.012

Zheng, X.-Y., Beard, B. L., Reddy, T. R., Roden, E. E., & Johnson, C. M. (2016). Abiologic silicon isotope fractionation between aqueous Si and Fe(III)–Si gel in simulated Archean seawater: Implications for Si isotope records in Precambrian sedimentary rocks. *Geochimica et Cosmochimica Acta*, *187*, 102–122. https://doi.org/10.1016/j.gca.2016.05.012

References From the Supporting Information

Young, E. D., Galy, A., & Nagahara, H. (2002). Kinetic and equilibrium mass-dependent isotope fractionation laws in nature and their geochemical and cosmochemical significance. *Geochimica et Cosmochimica Acta*, *66*(6), 1095–1104. https://doi.org/10.1016/s0016-7037(01)00832-8